AD-A110 872 APPLIED SCIENCE TECHNOLOGY INC ARLINGTON VA F/G 20/5
AN EXPERIMENTAL FACILITY FOR LASER/ACOUSTIC APPLICATIONS,(U)
NOV 81 G D HICKMAN, J A EDMONDS N00014-78-C-0784
UNCLASSIFIED AST-R-151181 NL

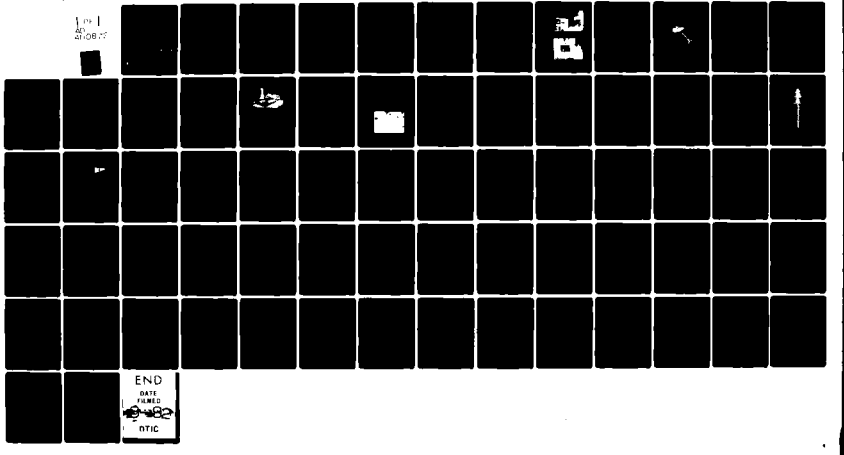

END
DATE FILMED
DTIC

AST-R-151181

AN EXPERIMENTAL FACILITY FOR LASER/ACOUSTIC APPLICATIONS

G. DANIEL HICKMAN
JOHN A. EDMONDS

TECHNICAL REPORT PREPARED UNDER CONTRACT N00014-78-C-0764

FOR

OFFICE OF NAVAL RESEARCH
COASTAL SCIENCES, CODE 422CS
ARLINGTON, VA 22217

NOVEMBER 1981

APPLIED SCIENCE TECHNOLOGY, INC.

1011 ARLINGTON BLVD. • ARLINGTON, VIRGINIA 22209 • 703-524-7081

3118 THOMAS DRIVE • PANAMA CITY, FLORIDA 32407 • 904-235-0327

TABLE OF CONTENTS

Abstract

This report describes the Experimental Laser/Acoustic System (ELAS) developed by Applied Science Technology, Inc., for applications involving the CO_2 laser/acoustic technique. This system is composed of a) a CO_2 laser transmitter to generate the acoustic signals in water, b) an acoustic receiving system, c) signal recording and analysis equipment, and d) a computer. A detailed description has been given for each of these subsystems. Laboratory and field measurements have used this system to investigate the feasibility of the laser/acoustic technique for remote sensing applications of a) shallow turbid water bathymetry, b) underwater object (mine) detection, and c) soil moisture determination. The ELAS is an extremely versatile system, as it is not tied to any specific transmitter or sensors. Therefore, there are numerous other applications involved with navigation and communication which this system could be used to investigate. Brief summaries of results obtained on the bathymetry, mine, and soil moisture programs are included.

Acknowledgments

The authors would like to thank Mr. Joe Green, a consultant to AST, Inc., who performed the calculations on the acoustic receiver. Drs. C. E. Bell and Bruce Maccabee of the Naval Weapons Center are gratefully acknowledged for their advice and help in assembling the equipment, in addition to participating in the Key West bathymetry experiments.

AN EXPERIMENTAL FACILITY FOR LASER/ACOUSTIC APPLICATIONS

1. Introduction

The pulsed infrared laser technique for generation of acoustic signals in water was demonstrated several years ago (Brewer, et al.; 1964; Carome, et al., 1966; Bell and Landt, 1967; Lowney and Sullivan, 1970; Bunkin, et al., 1971; Cawley and Bell, 1972; Maccabee and Bell, 1977). This technique consists of focusing an infrared laser, in our case a CO_2 laser - 10.6 μm, on the surface of water. Strong absorption of infrared energy by water limits the penetration of the beam to one or two wavelengths (10-20 microns). Evaporation of the water takes place as superheated steam if the pulse width is in the order of microseconds and the energy density of the laser spot on the water surface is sufficiently intense. The steam subsequently explodes, creating a shockwave both in the air and in the water. After approximately 0.5 μsecs, the shockwave in the water is reduced in velocity and the wavefront is transformed into a normal acoustic pressure wave. Acoustic pulses recorded within 1 meter of the explosion contain frequency components as high as 1 MHz. Pulses recorded at distances of tens of meters have frequency components as high as several hundred kilohertz. The majority of the pulse power, however, typically falls in the frequency range of 20-80 kHz, peaking between 25-30 kHz.

This technique for generating acoustic signals in water has several potential remote sensing applications in the hydrosphere and nearshore zone. Initial research by Applied Science Technology, Inc. has been directed towards two such applications--turbid water bathymetry and mine detection, and measurement of soil moisture. This research has been conducted under the sponsorship of the Office of Naval Research (N00014-78-C-0764). The first portion of the program was directed at assemblying a laser/acoustic system that could be universally used on these two applications as

well as numerous other applications such as: aircraft/submarine communication, submarine localization, and detection of the thermocline.

This report gives a complete description of the various components of our laser/acoustic system. Further discussion of our present acoustic air detection equipment and methods that are being investigated to improve this detection are given in Appendices A and B. Section 3 contains a brief summary of experiments and results obtained to date on the measurement of bathymetry.

2. Experimental Laser/Acoustic System (ELAS)

Applied Science Technology, Incorporated's experimental laser/acoustic system (ELAS) is used to generate laser acoustic signals, and to collect, analyze and plot experimental data. ELAS is comprised of a combination of standard off-the-shelf instrumentation and special control electronics designed by AST to integrate the various instruments into a complete laser/acoustic experimentation system.

The system block diagram is shown in Fig. 1. For purposes of our discussion, we can logically divide the system into the following four subsystems: a) laser, b) acoustic receiving system, c) signal recording and analysis equipment, and d) computer. These subsystems are described in the following paragraphs with particular reference to the bathymetry application.

Laser

A Lumonics model TEA-103-2 small aperture CO_2 laser capable of producing a one microsecond, 15 Joule pulse at a wavelength of 10.6 μm (infrared) is used as the transmitter. The laser is shown in Fig. 2(a). The laser beam exits from the black tube at the left side of the front face of the laser. A support beam (not shown) is bolted to the top of the laser housing and extended several feet beyond the front of the laser. A 45° gold mirror is mounted on an extension beam to direct the laser beam downward towards the water surface. A 40 inch focal length lens is placed in the path to focus the laser beam on the water, thereby increasing

SYSTEM CONFIGURATION

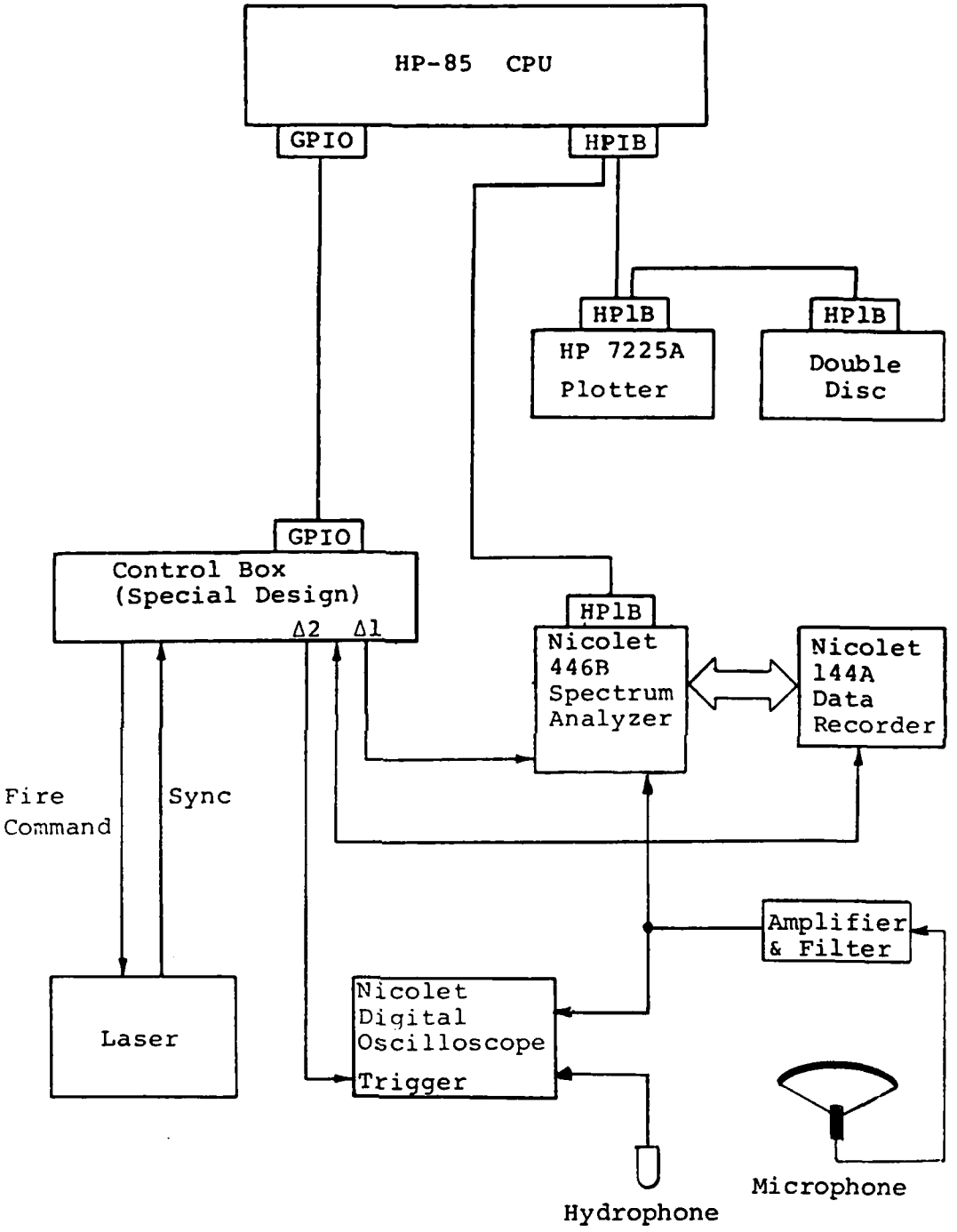

Figure 1: Hybrid Laser/Acoustic System Block Diagram

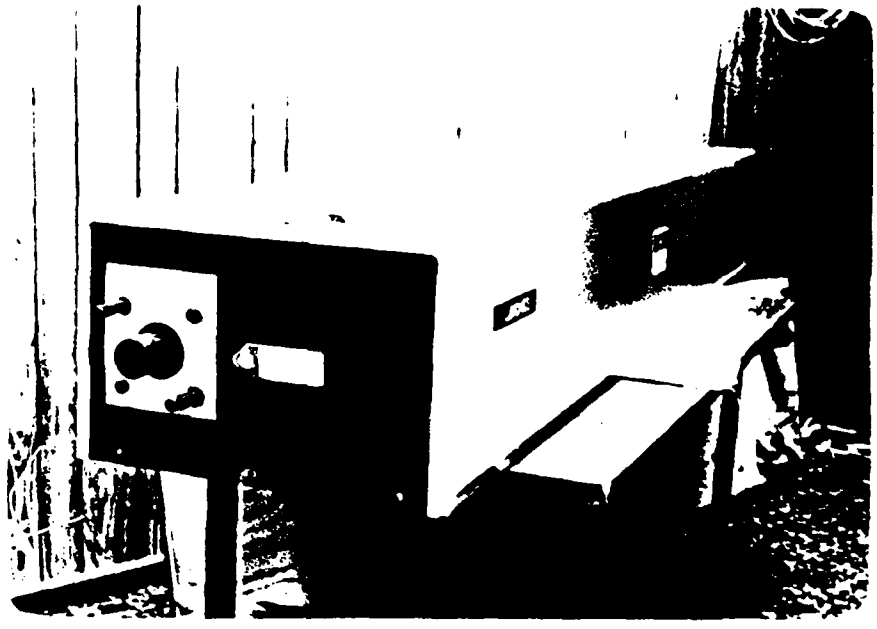

Figure 2(a): 15 Joule CO_2 Lumonics Laser

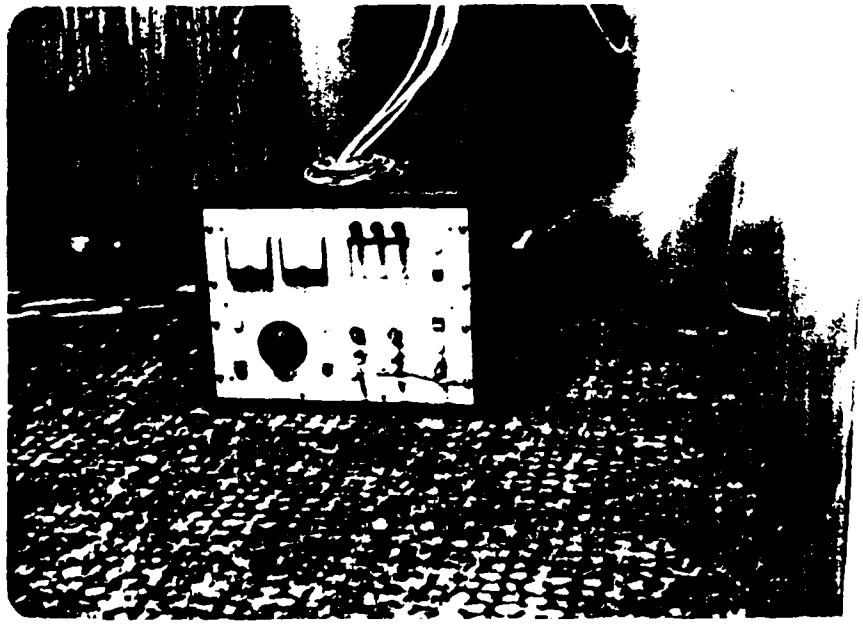

Figure 2(b): Laser Power Supply

the energy density. Air breakdown occurs, with subsequent reduction in the acoustic energy generated in the water, when the beam is brought to a focus in air above the water surface. Thus, focusing of the laser beam on the water surface becomes a critical aspect of this laser/acoustic technique for generation of acoustic pulses.

The laser power supply is shown in Fig. 2(b). This unit also contains the trigger control to fire the laser and the mixing valves for the laser gases. The laser may be triggered from an internal repetitive timer, front-panel push-button,or from an external source. There is a sync signal output which provides a high level electrical pulse at the instant the laser fires. Time-of-arrival measurements are referenced to this sync pulse.

In addition to the acoustic pulse generated in water, an acoustic signal is simultaneously generated in air. This is called the "air blast" and its presence must be considered in applying the laser/acoustic technique to remote sensing problems.

Acoustic Receiving System

Bathymetry experiments have been conducted using both hydrophones in water and microphones in air as acoustic sensors. The microphone-in-air technique is being pursued as a possible means of acquiring bathymetry data for turbid shallow waters without contact with the water. There are several problems associated with this technique which must be solved before a practical system can be implemented. These problems relate to the 65 dB signal loss at the water-air interface, platform noise and receiver flow noise. As an alternative, a small hydrophone could be deployed either from a sonobuoy or as a towed sensor.

AST has constructed an acoustic receiver to detect the return signal after passing through the water-air interface. The acoustic receiver consists of a Bruel and Kjaer (B&K) model 4149 (½ inch) microphone and a model 2619 preamplifier mounted in a 14 inch diameter parabolic reflector. The frequency response of the microphone is flat within ±2 dB between 3.9 kHz and 40 kHz. Its sensitivity is -38 dB re 1V/Pa. The reflector increases the sensitivity

by approximately 20 dB and provides a high degree of directivity. The acoustic receiver is shown in Fig. 3. The microphone is mounted at the center of the tripod support which is seen extending downward from the reflector. The acoustic receiver is mounted at the end of an extendable boom. A mounting plate is provided to attach the boom to the ship. The boom is adjustable in length and orientation. The receiver mount is articulated so that the receiver may be pointed at any angle with the water, fore and aft and side to side.

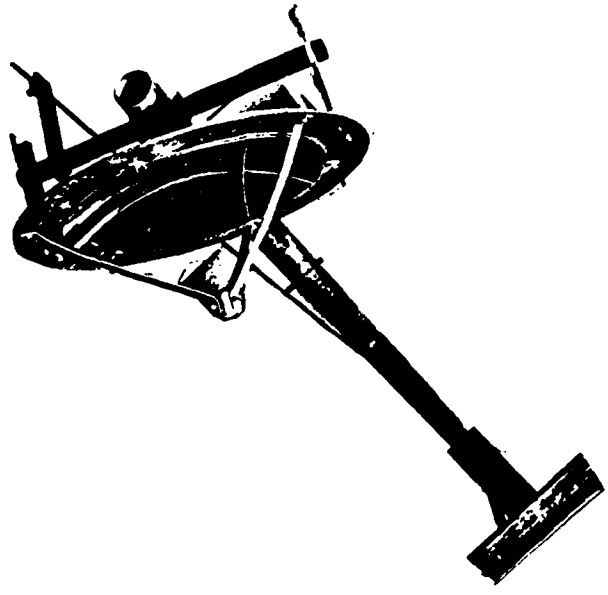

Figure 3: Acoustic Receiver

The power supply (B&K model 2807) for the microphone preamplifier includes a unity gain signal amplifier for driving low impedance coax cables. The signal path is from the microphone preamplifier to a 20 dB gain amplifier, a tunable band pass filter, a Hewlett-Packard 450AR amplifier (20/40 dB gain) and to the Nicolet 446B spectrum analyzer.

The tunable filter is a Krohn-Hite model 3202 active filter. It contains two independent, four-pole filters, each of which can

be used as either a high or low pass filter. Bandpass and band-reject characteristics can be obtained by cascading the two filters. The filter is used to reduce out-of-band signals and noise. The filter has a gain of 0 dB in the passband.

The sensitivity of the acoustic receiving system can be calculated: The system sensitivity at the input to the spectrum analyzer =

-38 dB re 1V/Pa (microphone)
+20 dB (reflector gain)
+20 dB (amplifier gain)
+40 dB (HP 450A amplifier gain)
=42 dB re 1V/Pa = -78 dB re 1V/μPa

The receiver is calibrated using the setup shown in Fig. 4. A test is made to determine the optimum position of the microphone in the reflector. Using a test tone of 24 kHz, the microphone is moved along the axis and the signal amplitude of the signal is monitored. The microphone is locked in at the position giving the highest output amplitude. A measurement is then made to determine the gain vs. frequency calibration for the acoustic receiver. At each test frequency, the output of the microphone placed in the reflector is compared with the output of the microphone without the reflector. The analyzer is used in the averaging mode (16 summation averages per reading) to reduce the adverse effects of wind and ambient noises.

The hydrophone is a B&K model 8103 and is used in conjunction with a model 2635 conditioning amplifier. The response of the hydrophone is flat (±2 dB) from 1 Hz to 80 kHz. The sensitivity of the 8103 with the 2635 is adjustable in 10 dB steps from -120 to -200 dB re 1V/μPa. The amplifiers and filters described above for the microphone are also usable with the hydrophone when necessary.

Signal Recording and Analysis Equipment

The signal recording and analysis equipment includes:

a) Nicolet Scientific model 446B real-time spectrum analyzer,

b) Nicolet Scientific model 144 data recorder,

c) Nicolet Scientific Explorer II digital oscilloscope, and
d) special control electronics designed by AST, Inc., to interface the Nicolet equipment and the laser with the computer system and to provide event time synchronization.

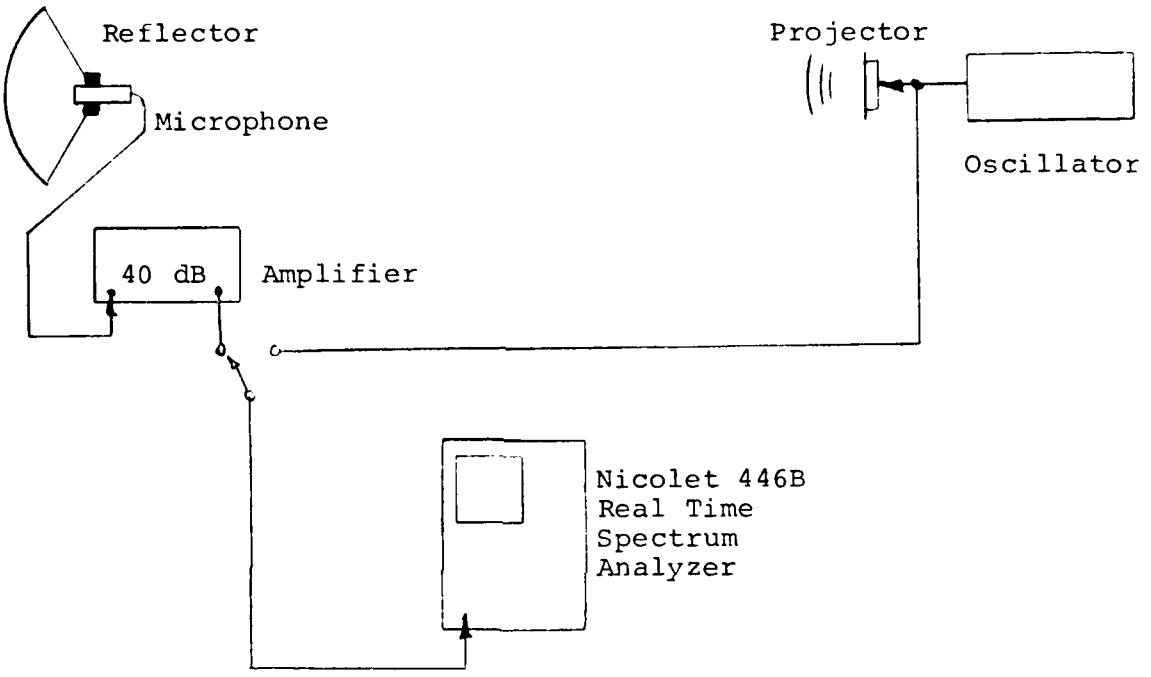

Figure 4: Acoustic Receiver Calibration Test Setup

The Nicolet 446B is a real time spectrum analyzer which performs a digital Fast Fourier Transform (FFT) of digitized time domain signal data to obtain the frequency spectrum of the incoming signal. The frequency spectrum covered by the Nicolet 446B extends from DC to 100 kHz. Since the frequency response of the microphone is limited to 40 kHz and the return pulse spectrum is in the 25-40 kHz region, the optimum spectrum analyzer operating range is the 50 kHz range. The 50 kHz and 100 kHz ranges encompass the entire microphone spectrum, but the 50 kHz range provides a wider analysis time window (8 ms). The maximum input sensitivity of the analyzer is obtained using the 100 mV RMS setting. This results in a display range of $\pm$140 mV in the time mode.

In addition to the time mode, the frequency spectrum of the signal may be displayed. There are also several averaging and trigger modes available.

Because the expected input signal is a short duration pulse displaced in time from the initiating laser pulse, the analyzer is triggered externally by the Special Control Electronics (SCE). When using the 50 kHz range, one millisecond of pretrigger time data plus seven milliseconds of post-trigger time data is stored and displayed by the analyzer as a sequence of 1024 equally spaced (in time representation) digitized signal level values, with an amplitude resolution of 12 bits.

The analyzer is connected to the Model 144 data recorder via a high-speed parallel data bus. The displayed time data can be recorded on command from the computer by actuating a front panel push button. The data recording is accomplished in slightly under one half second. Approximately 1000 such data images may be stored on one 3M model 300 A magnetic tape cartridge. Each image is identified with a unique tape file number. All of the spectrum analyzer front panel settings are also recorded on the tape.

The data may be retrieved from the tape by dialing in the appropriate tape file number and transferring the data back into the analyzer. The analyzer can compute the spectrum of any signal retrieved from the data tape.

The spectrum analyzer may be controlled by the HP-85 computer via the standard HP Interface Bus (HP-IB, IEEE 488). Time and spectrum data may be transferred, in either direction, between the computer and analyzer via the HP-IB. Only the external trigger is supplied by another source--the SCE.

The block diagram for the SCE is shown in Fig. 5. The SCE interacts with the HP-85 computer via the HP General Purpose Interface Bus (GPIB) and has four basic functions:

a) interface the laser trigger input to the computer,
b) accept the laser sync pulse as a start pulse for the trigger delay timer,
c) provide two independent and controllable (manual and computer) trigger delays for the spectrum analyzer and the digital scope, and

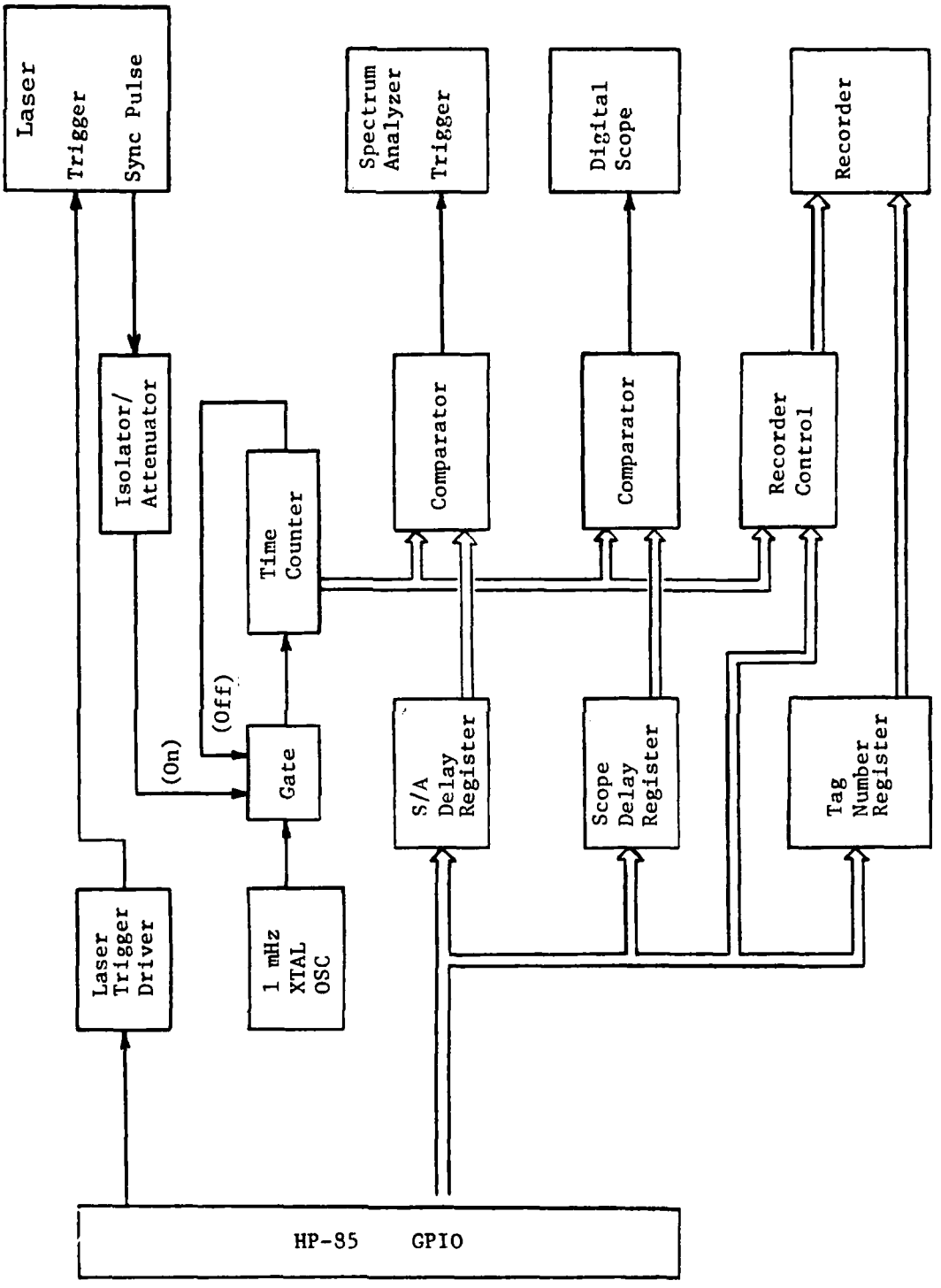

Figure 5: Block Diagram, Special Control Electronics

d) control the data recorder.

Since the laser operation requires the switching of high energy, short duration pulses (40 kV, 1 μs) care must be taken to avoid either radiated or conducted electromagnetic interference. For this reason, both the laser trigger input and the sync output are electrically isolated from the SCE. The command pulse from the computer goes to a relay driver circuit in the SCE. This in turn operates a relay at the laser; the relay contact closure triggers the laser. The 50 V sync pulse from the laser is isolated from the SCE logic circuitry by means of an optically coupled isolator (optocoupler).

The SCE uses a 1 MHz crystal controlled oscillator and a six decade counter as an elapsed time counter. The counter is started upon receipt of the laser sync pulse and is stopped on completion of exactly one second elapsed time. The desired spectrum analyzer trigger delay time is preset in a two digit storage register (units and tens of milliseconds) by the HP-85 computer. A digital comparator generates the trigger pulse when the value of the elapsed time counter equals the preset register value.

The oscilloscope trigger delay circuit is identical to that for the spectrum analyzer. Also, there is a provision for each to be operated manually from push button switches on the front panel.

The time counter also controls the time sequence for controlling the digital recorder, and for sensing errors in the laser firing and data recording cycles.

Computer

The Hewlett-Packard model 85 computer is a so-called "personal size" computer well suited for scientific applications. The HP-85 benefits from its ease of interfacing with other instrumentation, available peripheral devices and support software. The computer is comprised of:

a) HP-85 computer with built in CRT, magnetic tape drive and thermal alphanumeric printer,
b) 32K Random Access Memory (RAM),
c) Model 82901M Dual Disc Drive,

d) Model 7225B Graphic Plotter,
e) Basic programming language,
f) HP-IB (IEEE-488) and General Purpose Input/Output (GPIO) interfaces.

The HP-85 computer is used to control the laser and the signal analysis and data recording equipment during the field measurements, and to perform post-experiment analysis of the data. Figure 6 shows the computer, plotter, floppy disc drive unit, spectrum analyzer data recorder and the Special Control Electronics (SCE). Other electronics used but not shown include the B&K microphone power supply and the signal amplifier and filter.

Experiment Mode. In the experiment mode, the computer serves several functions: a) to control and synchronize the operation of the laser and signal analysis equipment, b) to provide on-line computation of depth (bathymetry application) from the return pulse data, and c) to assist with the data recording chores.

A computer program combining these functions was written by AST, Inc. The program allows the test operator to enter record keeping data such as date, time, disc I.D. number and tape I.D. numbers. This data serves to coordinate the record keeping between the laboratory book, computer disc and Nicolet data recorder.

In addition, the operator can select test conditions such as:
a) laser firing mode,
b) record the spectrum analyzer data on magnetic tape (yes, no),
c) automatic or manual control of the spectrum analyzer trigger delay,
d) geometric constants for depth calculation,
e) X-Y plot of depth, and
f) storage of depth data on disc.

There are three laser firing modes to choose from: "Manual," "automatic" and "off." In the "manual" mode, the operator may fire the laser at will by actuating a special function key on the computer. The laser must not be fired more frequently than once every two seconds when operated at high output levels. The data aquisition,

storage and computation procedures exceed this figure and thus prevent the laser from being fired too rapidly.

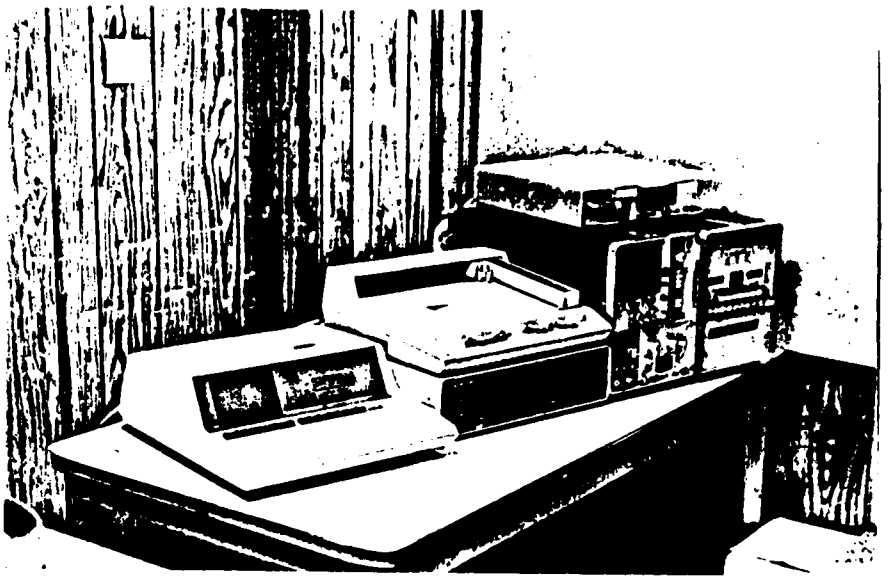

Figure 6: Computer, Plotter, Floppy Disc Drive Unit, Spectrum Analyzer Data Recorder and the Special Control Electronics (SCE).

In the "automatic" fire mode, the operator may select a specific additional time interval for retriggering the laser. The computer's internal timer issues the firing command. This mode is useful when making repetitive measurements. The "off" mode prevents the computer from firing the laser when someone is working on the laser, i.e., aligning the optics etc.

The operator may type the spectrum analyzer and oscilloscope delay values into the computer. These values are then transmitted to the SCE trigger delay circuit. Each time the laser fires, the delay values are read back to the computer to assure that the display is current and that the computations performed will use the correct values. The operator may also adjust the delay value using the special function keys on the computer. The delay value is incremented one millisecond each time the "UP" key is actuated, and decremented one millisecond each time the "DOWN" key is actuated.

The operator may select an automatic trigger mode. In this mode the computer reads the spectrum analyzer data and searches for the bottom return pulse (bathymetry application) using a threshold detection algorithm. The threshold level can be adjusted by the operator. The algorithm computes the time of arrival of the bottom return by adding the preset trigger delay to the time difference between the trigger and the detected return pulse. The computer then sets the trigger delay for the next pulse so that the return pulse from the next laser shot will occur within one millisecond of the trigger point (assuming no change in depth). This method gives satisfactory results for most depth profiles encountered.

The return pulse detection algorithm also includes a depth calculation. The operator must key in the constants relating to the horizontal separation distance of the microphone to the laser and the height of the microphone above the water. The calculated depth is displayed on the CRT along with time, shot number, tape file number and trigger delay value. The screen data may be printed on the HP-85 alphanumeric printer or stored on disc at the option of the operator. Also, depth vs. shot number may be plotted on the HP-7225B plotter.

The time to execute the depth algorithm is dependent on the number of data points (1024 maximum) the computer must examine before detecting a threshold crossing. Typically, this time is on the order of five to ten seconds. The laser cannot be re-fired until the computation has been completed.

Analysis Mode. The HP-85 has been programmed to assist in the post-analysis of the experimental data. There are two objectives: a) the computation of depth and comparison with the fathometer readings, and b) the determination of the frequency spectrum of both the background noise and the bottom return pulse.

Using the computer, the analyst can select any point in the spectrum time record for a given laser shot and a) determine its amplitude and time of occurrence, b) create an X-Y plot of the time record, c) create an expanded X-Y plot of one millisecond window around the return pulse, and d) "edit" the background noise out of

the time plot, then return the editted data to the spectrum analyzer to obtain the frequency spectrum of the pulse alone.

Mobile Van Facility

AST, Inc. has acquired the maxi-van (shown in the following picture) to house the laser, computer and associated electronics described in Section 2. The van is equipped with a motor generator which will enable the equipment to be transported to any remote site and operated independently. For our next shipborne measurements, the fully equipped van will be driven aboard the LCU landing craft. During the measurements, the ship's engines will be turned off and the equipment will be operated from the motor generator. Operating in this mode will greatly reduce some of the noise and ground-loop problems experienced during our initial shipborne experiments where we operated using the ship's power.

This mobile facility will also enable us to continue our soil moisture measurement by going to isolated beaches to avoid interference from nearby structures and spurious sources.

Mobile Van Facility

3. Applications

Bathymetry

Rapid surveillance of inshore waters has drawn the attention during the past several years of the U.S. Navy and Marine Corps as well as civilian agencies such as the National Ocean Survey (NOS), the U.S. Geological Survey, the Corps of Engineers and the National Aeronautics and Space Administration. Remote detection and mapping of water depths (bathymetry) still remains one of the unsolved problem areas of inshore mapping.

Extensive research has been made using pulsed blue-green lasers (LIDARS) to map shallow water depths from aircraft. The results of this work led to the development of several prototype systems. These systems have proven to be accurate, having high mapping rate capability for shallow waters. However, optical LIDAR systems are severely limited by water turbidity. In a good portion of the coastal zones of the world, turbidity would limit airborne LIDAR mapping to water depths shallower than 30 feet. For instance, typical Chesapeake Bay type waters would probably limit this technique to 10 feet or less.

Boat-mounted side-scan sonar (acoustic) systems for shallow water bathymetric mapping have been developed to a high degree of sophistication. However, these systems have been designed to operate with both the transmitter and receiver located in the water. Therefore, data acquisition rates are limited to those that can be obtained by slow survey boats (6-10 knots).

A technical assessment program was initiated (Hickman, 1975) to determine the feasibility of using an airborne acoustic (transmitter and receiver) system for rapidly mapping bathymetry of highly turbid shallow waters ($\leq$30 feet). This technique, which could be used in conjunction with the blue-green LIDAR system, would have its greatest value in mapping waters in which the optical LIDAR system is severely limited by the water turbidity. Estimates have been made that at least 15% (probably greater) of the coastal areas can be classified as highly turbid.

It is anticipated that such an airborne acoustic system, if proven feasible, would be flown on either surface effect ships or

helicopters at speeds up to approximately 100 knots (See Fig. 7). The data rate would be at least 10 times larger than that obtained by small boats towing conventional sonar equipment. In addition to the increased data rates available from these platforms, areas could be surveyed, that due to their inaccessibility and possible hazards to small boats, have not been surveyed.

The acoustic field that is created in water by the CO_2 laser penetrates the medium and is reflected off objects and the bottom sediment. A portion of this energy is reflected back towards the air/water interface. The return acoustic signal, if of sufficient energy, is detected with a microphone in the air (See Fig. 8).

The water depth is determined from a measurement of the total transit time (t_T) of the acoustic pulse from the spot of generation at the water surface to the bottom sediment and back to the receiver located in air. The water depth (d) is calculated using Equation 1.

$$d = \tfrac{1}{2}\left[V_w^2 (t_T - h/V_a)^2 - (a)^2 \right]^{\frac{1}{2}} \qquad (1)$$

where a is the horizontal distance between the laser, and V_w and V_a are the acoustic velocities in water and air respectively.

In addition to the acoustic pulse generated in the water, an acoustic pulse is simultaneously produced in air. This "air blast" travels along path b (Fig. 8) to the microphone receiver. The attenuation of the air blast is much less than that of the acoustic bathymetric signal emerging from the water. Therefore, if the air blast is detected simultaneously with the arrival of the "signal" pulse, the air blast will mask the signal. However, the velocity of sound in water is approximately five times faster than that in air. Using this fact, the distance between the laser and receiver can be adjusted so that the "true signal" reflected from the bottom sediment, arrives at the receiver prior to the arrival of the air blast.

The bathymetry program is currently in the experimental phase. AST, Inc. is presently conducting field tests that are designed to

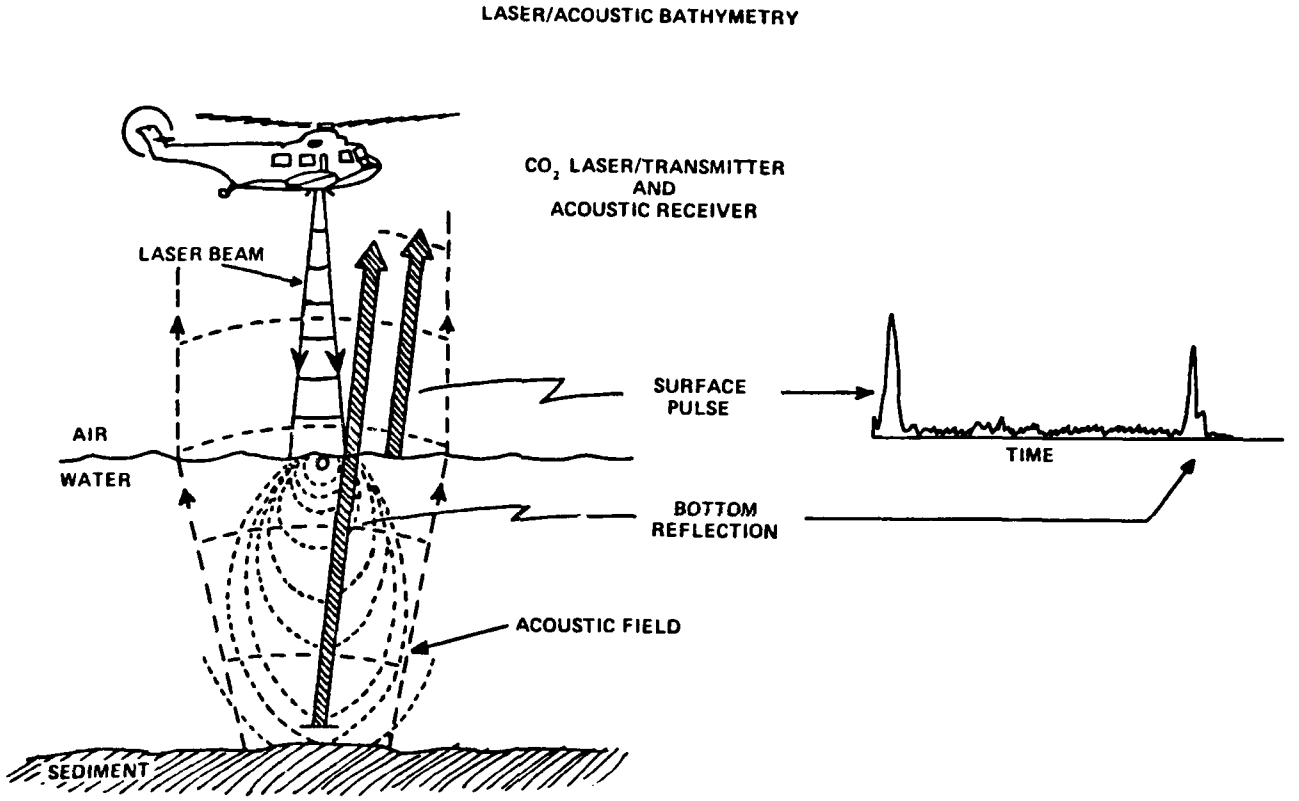

Figure 7: Laser/Acoustic Bathymetry

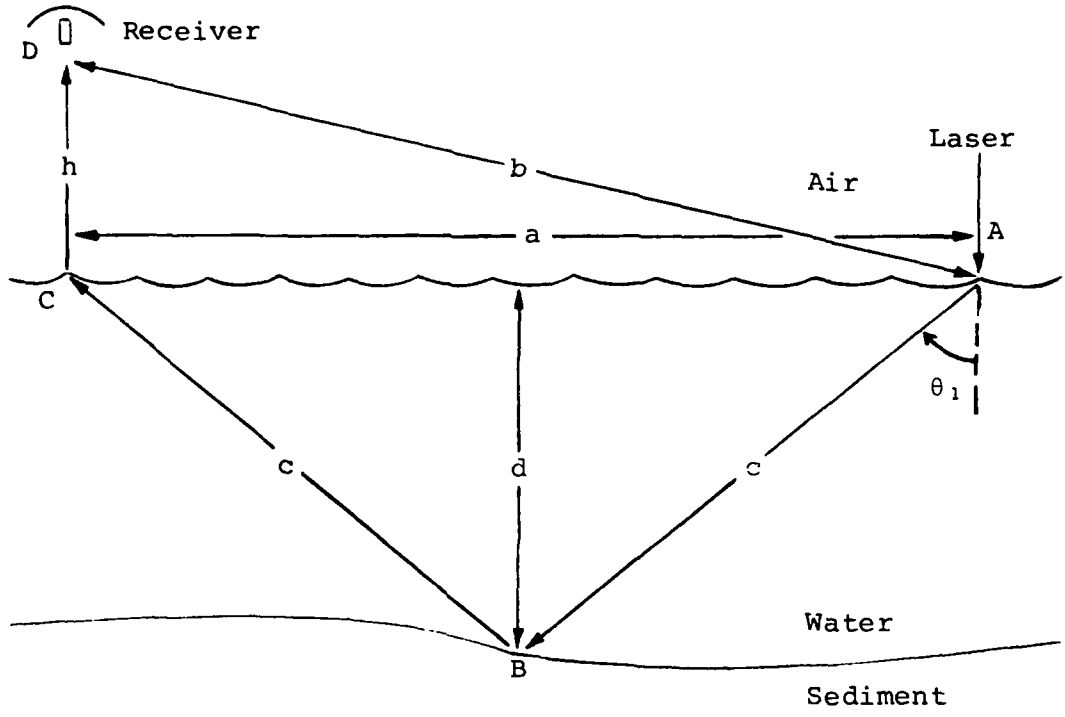

a = laser to microphone straight line horizontal distance
d = depth of water
c = acoustic path in water, surface to bottom (total path in water = 2c)
b = air blast path, laser to microphone
h = elevation of the receiver above the water
θ_1 = acoustic path angle

Figure 8: Signal Path Geometry

investigate the problems associated with applying the laser/acoustic technique to remote sensing of bathymetry and underwater object detection. The initial feasibility experiments were performed at the Navy's Brighton Dam Reservoir facility in Maryland (Hickman, et al., 1980). These tests were performed from a floating dock in very quiet waters. The results of these measurements were extremely encouraging for both turbid water bathymetry and underwater object detection. Measurement of water depths as great as 20 meters was made using a microphone to detect the acoustic signals in air. In addition, a MK-84 mine lying on the bottom (depth ≈ 20 meters) was distinguishable from the sediment reflection. The results proved that the CO_2 laser system can be used to generate acoustic signals in water of sufficient intensity to be detected in the air, after being reflected from sediment in shallow water. It may be also possible to use the spectral analysis of the reflected acoustic pulses as a measure of the hardness and type of bottom sediment.

A second set of experiments were designed to test the concept of the laser/acoustic-technique for bathymetry under operating conditions of a ship in the real environment. These tests were carried out during the summer of 1981 from a U.S. Navy ship, the LCU-1614, a landing craft, maintained and operated by the Naval Air Development Center at Key West, Florida.

Figure 9 is a test plot of the acoustic signals made with the system at a pool. The signals were recorded by the spectrum analyzer and HP-85 computer and printer by the X-Y plotter. The indicated depth of 10 feet was obtained. Of notice is the low noise in relation to the strong signal return. Figure 10 is a typical plot of signals recorded aboard the ship at Key West. The initial pulse is the reflected signal from the bottom sediment and indicates a water depth of 23 feet. The air blast is shown to arrive 3.5 msecs after arrival of the bathymetric signal. The recorded noise, in this case, is appreciably greater than observed for the pool experiments. The noise is, of course, a limiting factor in this technique and is discussed in more detail later.

Calculation of the time it takes the air blast to reach the receiver, and the maximum depth that could be measured for each of

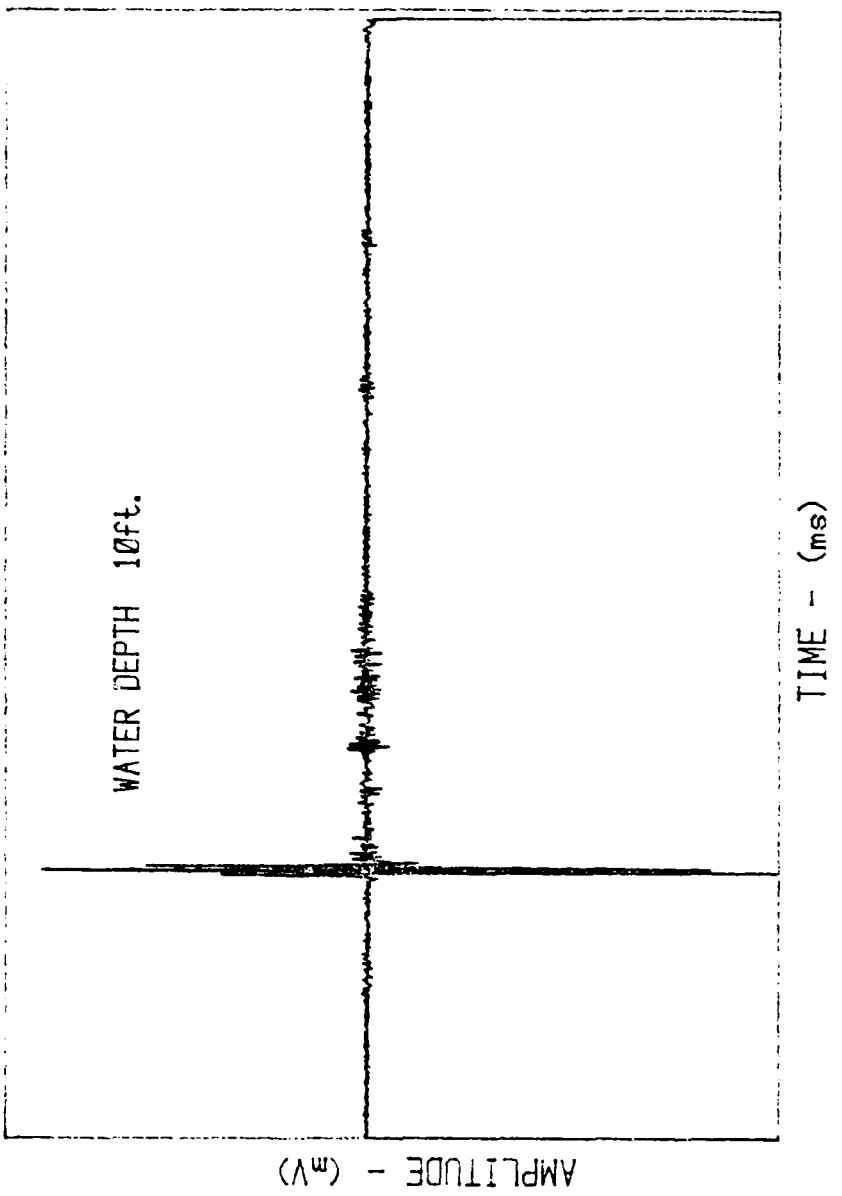

Figure 9: Laser/Acoustic Returns
Pool Experiments

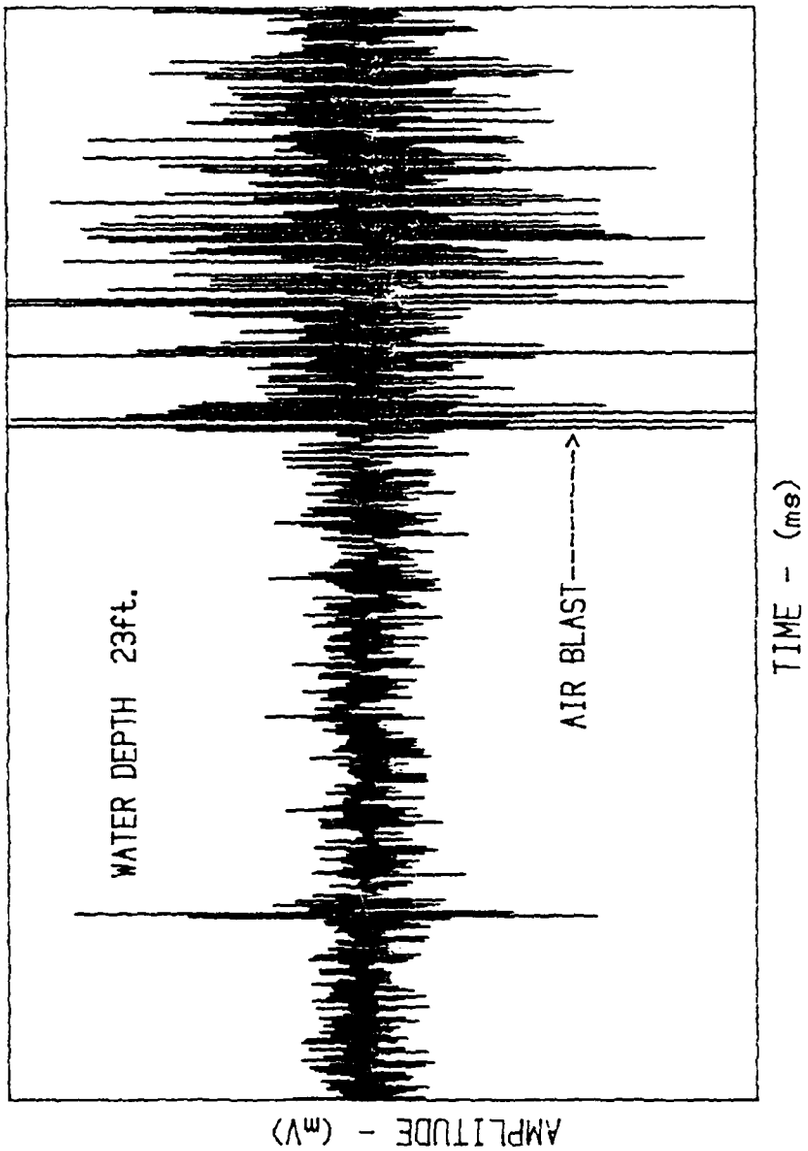

Figure 10: Laser/Acoustic Returns
Key West - August 1981

the Key West test conditions, i.e., signal arriving prior to air blast, are presented in Table 1.

Table 1: Test Configuration Parameters

Configuration	h (meters)	a (meters)	Air Blast time (ms.)	Max. Depth* (meters)	Transmission Loss (dB)*
A	3.4	17.2	50.9	20.7	36.0
B	4.3	11.3	35.2	16.8	31.1
C	2.7	26.3	76.7	51.5	40.6
D	3.8	16.7	49.7	28.9	35.6

* For air blast limited case

The signal attenuation in water is due mainly to spherical spreading. An additional loss of signal is encountered due to the fact that the acoustic source generated in water has an angular dependence which has been measured as $\approx \cos\theta$. This transmission loss (TL) through the water is calculated as:

$$TL = 20 \log (2c) - 20 \log(\cos \theta_1)$$ (See Table 1 & Fig. 8)

Figure 11 is a plot of transmission loss vs. water depth for the various microphone-laser separations used on the ship. Zero separation (microphone directly above the laser) yields the lowest values for transmission loss at all depths. However, the interference from the air blast prevents co-location of the laser and the receiver. Transmission loss increases as the separation distance increases. The maximum separation possible using the LCU-1614 is 45 meters, while the actual separations used ranged between 10.2 and 26.3 meters. The shaded area in Fig. 11 indicates the range of operation for the Key West experiments.

The depths encountered during the Key West experiments ranged from just under 20 feet to about 70 feet (7 to 21m). The transmission loss experienced by the acoustic signals in the experiments

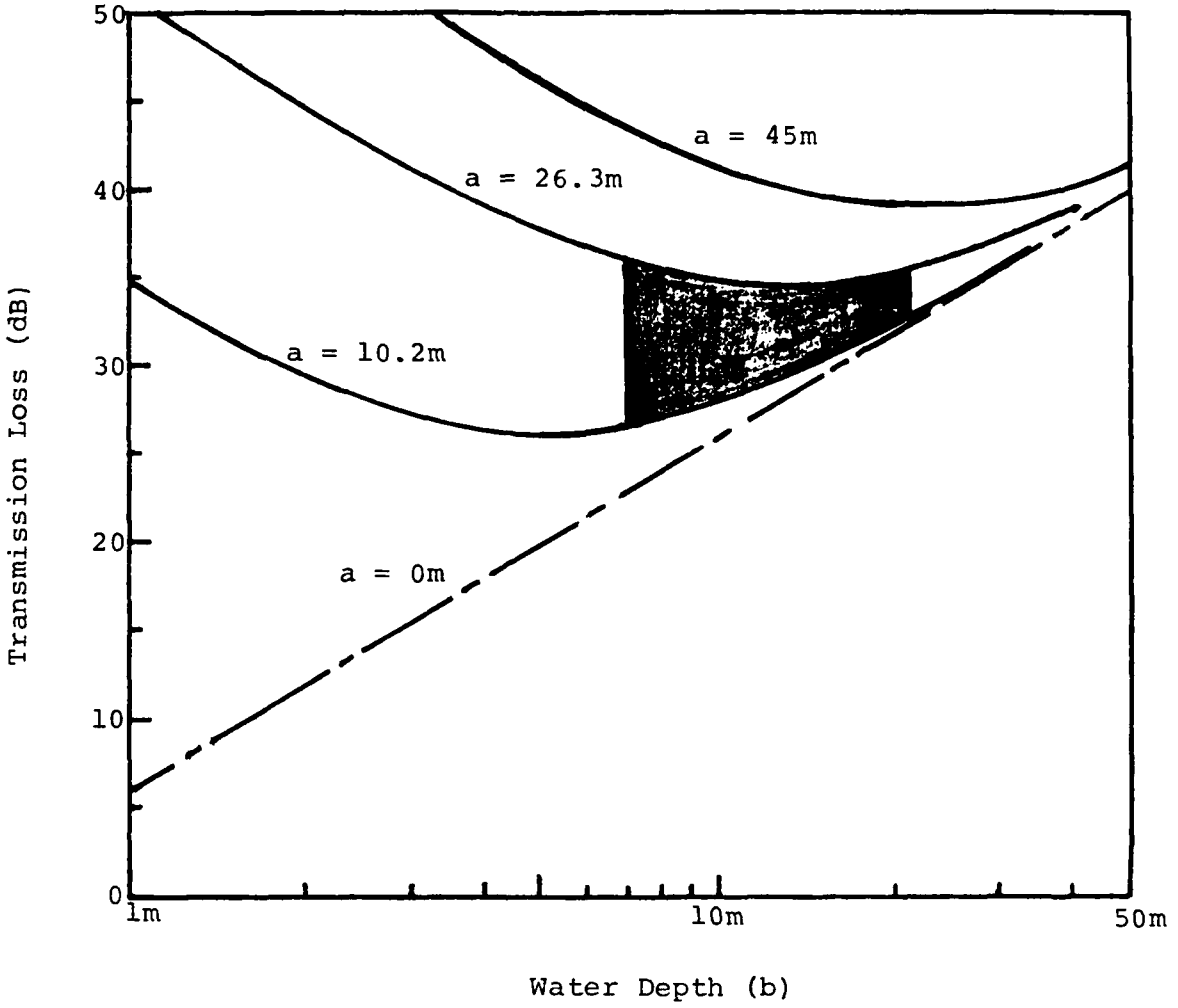

Notes:

1) a is the separation distance between the microphone and the laser
2) Transmission loss shown includes source directivity and spherical spreading loss. It does not include bottom reflectivity or water-air interface losses.
3) The shaded area represents the operating range for this experiment.

Figure 11: Transmission Loss vs. Water Depth as a Function of Microphone-Laser Separation Distance.

ranged from 27 to 36 dB. There was an additional measured loss of approximately 23 dB due to the reflectivity of the bottom sediment. The signal is further attenuated at the water-air interface by 65 dB. Therefore, the total signal loss for these water depths, assuming a calm and smooth water surface, ranged from 115-124 dB. Since the laser generated SPL in water was measured as approximately 195 dB re 1 μPa, the expected SPL at the microphone should be in the range of 71 to 80 dB re 1 μPa. This corresponds to an observed signal on the spectrum analyzer of between 0.5 V and 1.3 V. The signals observed were typically of smaller intensity.

The motion of the ocean waves has two effects on the received signal strength. First, the wave heights, which generally ranged between one and two feet high, affected the SPL of the generated acoustic pulse. The spot size, and therefore the energy density, varied widely as the distance between the lens (40 inch focal length) and water varied. The SPL generated in the water is also affected by the angle of incidence of the laser beam with respect to the wave surface, and the relative placement of the spot on the wave.

Secondly, the waves present a constantly varying surface orientation in the acoustic receiver's field of view. The refraction at the water-air interface limits the angle at which sound exits from the water to a 26° cone whose axis is normal to the surface. The narrow beam pattern of the acoustic receiver ($\simeq 1^{\circ}$) results in a target area on the water of about a 6 inch diameter or less for the given height of the microphone and the water depths investigated. Because the beam pattern of the present acoustic receiver cannot be guaranteed to be in alignment with the direction of the signal emerging from the water, one can expect substantial variations in the intensities of the signals. Possible solutions to this problem are discussed in Appendix B.

The wave motion, therefore, results in a wide range of signal levels, and a receiver having a wide dynamic range would be desirable. The dynamic range for a receiver is limited at low signal levels by receiver generated noise. The noise levels observed at the spectrum analyzer were typically in the range of 60 to 100 mV

P-P, with unexplained noise spikes reaching 2-3 times the average noise level.

One of the most critical noise sources is that associated with the platform, i.e., intrinsic platform noise, and that caused by receiver flow noise. Spectral noise signatures of various platforms are being investigated to determine the noise as a function of frequency. One of the advantages of operating a receiver in the frequency range 30-40 kHz is that in general, aircraft noise decreases with increasing frequency. The exact noise figures are as yet undetermined. Additional experiments are required to determine the best configuration for the acoustic receiver, in order to minimize air flow noise, the temporary overload of the microphone system caused by the air blast, and aircraft background noise. It is possible that a noise cancelling microphone array and/or a highly directive system can be used to minimize this background noise, while maximizing the sensitivity of the receiver to the bottom echo.

Good results on bathymetry were obtained from the Key West experiments. However, there are a number of areas where substantial improvements will be made prior to the next set of shipborne measurements. A brief outline of the problems and improvements being made is given below.

- Noise - both the environmental and equipment noise were higher than anticipated. To overcome the major sources of noise the following modifications are being made: a) microphone and receiver shielded with acoustic foam; b) use of an amplifier having a smaller noise figure; and c) use of motor generator to allow the ELAS to be operated independent of ship power.
- Transmitter - the techniques used to focus the CO_2 laser on the water surface caused considerable trouble. An improved design for a laser telescope is being investigated. The lens combination of this telescope will have a longer focal lens. This will allow the system to be operated from a greater distance from the water.
- Receiver - the small acceptance angle of the microphone-collector system ($\simeq 1^{\circ}$) caused problems in pointing the

reflector in the "right" direction for detection. This problem is thought mainly to be due to wave action. Several alternatives for receiving the acoustic signal in air are being considered. These alternatives are described in Appendices A and B.

In conclusion, the results obtained to date have shown that a "complete" airborne laser/acoustic mapping system for shallow water turbidity is feasible. Also, with increased laser energy it should be possible to increase the depth measuring capability of the system. For instance, the Sound Pressure Level (SPL) from 200m depths should be comparable to that detected in the present experiments (i.e., ≈ 76 dB), if the laser energy density is increased from 5 to 50 Joules/cm^2. If the bottom strength is reduced to -20 dB, the bottom echo of 75 dB from a water depth of 200m would be obtainable by increasing the laser energy density to 150 Joules/cm^2. Based on state-of-the-art TEA lasers, it appears that lasers and optical systems could be designed to create surface energy densities as great as 150 J/cm^2 using largely "off-the-shelf" items.

Mine Detection

In addition to bathymetry, our experiments have shown that it may be possible to detect underwater objects, such as mines, close to and in some cases lying on or buried in the sediment. Our initial experiments performed at Brighton Dam in Maryland were able to distinguish a MK-84 mine on the bottom (depth of water ≈ 20 meters). The measurements used the microphone in the air to detect the acoustic reflection from the mine.

A series of experiments is being designed to further investigate the feasibility of using laser/acoustics for detection and identification of mines. It is planned to perform these experiments in the waters near the Naval Coastal Systems Center, although it may be more advantageous to make the measurements at Key West, Florida.

If possible, the specific site for making the measurements will be one in which the mine(s) can be easily lowered from the

surface to the bottom and even buried in the sediment, and where the water depth varies from a few feet out to 50-100 feet. The CO_2 laser will be set up so that the beam can be easily focused on the water surface. Detection of the acoustic signal reflected from the sediment and the mines will be made using both hydrophones in the water and a microphone receiver in air. The data will be recorded on a spectrum analyzer, stored on magnetic tape, and analyzed by the HP-85 computer.

The primary interest in these experiments is to determine the mine reflectivity/sediment reverberation ratio for various mines. This ratio will be determined as a function of water depth and location of the mine with respect to the bottom sediment, the laser transmitter and the receiver. In addition, a detailed analysis will be made of the frequency spectrum of the acoustic signals reflected from the mines and that reflected from the sediment. The initial experiments performed at Brighton Dam with a MK-84 mine indicated that large differences might exist in these spectra. If such is the case, spectral analysis of the reflected signals could aid significantly in discriminating objects close to and buried in the sediment.

Soil Moisture and Trafficability

The success or failure of a military operation is highly dependent on the ability of the ground forces to move from Point A to Point B within time constraints dictated by the particular battlefield situation. An amphibious assault force must be concerned with the determination of where to go ashore and, once there, the possible routes inland. It is also essential to know the mobility options open to the enemy.

Modern day battlefield tactics call for early identification of enemy thrusts, and a rapid movement of forces. A thorough knowledge of the conditions affecting mobility throughout the battlefield area would give the commander a decided advantage in planning the movement and placement of his own forces while denying enemy access to routes most advantageous to them. Not only is mobility to be considered in pre-planning a military operation,

the dynamic nature of the battlefield demands that the current status and accurate short term predictions of mobility be available during the course of battle.

For several decades, research has been conducted into the various aspects of cross country mobility (CCM), i.e., the ability of the terrain and the environment to allow traversal by military vehicles. These efforts have been applied to the two complementary aspects of the problem--the development of vehicle designs which enable mobility across expected terrain impedances, and the acquisition of geographic intelligence from which battlefield mobility may be ascertained. The research has led to the quantification of many of the factors which determine CCM. This facilitates the use of computer models for vehicle design and battlefield mobility assessment.

Vehicular attributes such as ground pressure, suspension characteristics, power, speed, accelleration, load, traction, visibility, and driver accelleration (bounce) are readily quantifiable. Research has provided an empirical basis for quantifying terrain impedance factors for simulation purposes. CCM modeling is now an important step in the development and evaluation of military vehicles.

To assess mobility in a specific battlefield environment, information must be gathered regarding land use, vegetation, terrain features, geology, hydrology and trafficability. Weather data is also needed for predicting changes from the current status. The object of the assessment is to map the areas which are impassable to the vehicle types employed, and to identify those areas which will permit the flow of military vehicle traffic. Further, the rate of speed which can be attained is to be estimated as well.

Some of the required data can be obtained from aerial photoreconnaissance, radar or other remote sensors, existing maps and, where possible, from *in-situ* measurements. Trafficability--the capacity of a soil to permit traffic by vehicles--is a major factor of CCM and has been difficult if not impossible to determine by remote sensing techniques. *In-situ* measurement of soil strength is usually performed manually using a cone penetrometer. This

technique has been adapted for remote sensing of soil strength through the use of air-droppable penetrometers. This method has some obvious drawbacks. A truly remote sensing capability is an important, yet unsatisfied battlefield systems requirement.

The problems of mobility experienced in World War II, the Korean Conflict and Viet Nam has motivated research investigations of soil properties and into the performance of military vehicles travelling over a variety of soil types and conditions. Parallel efforts in soil research directed towards solving agricultural, land use, and other related problems have also contributed to the understanding and measurements of the trafficability of soils.

To be trafficable, a soil must exhibit (a) sufficient load bearing capacity to support the vehicle without excessive sinkage, and (b) sufficient traction capacity to enable the vehicle to overcome its rolling resistance and move forward. Bearing and traction capacities are both functions of the shear strength of the soil. Soil strength is related to its moisture content, mineralogic and organic composition, grain size and shape, plasticity and density. Soil moisture is the predominant factor affecting trafficability. In general, as the moisture content is a given soil increases, its shear strength decreases.

AST, Inc. made a survey and technical assessment of the various sensors and techniques used to detect and map soil moisture. The results of this study are given in two publications: Hickman et al., 1981; Edmonds and Hickman, 1981. In summary, microwave sensors have the greatest potential for measuring soil moisture by remote means. Passive microwave is less expensive and easier to operate than active (radar) sensors. Radar can achieve much greater spatial resolution than passive microwave radiometers. Spatial resolution is an important factor in mapping trafficable soils. Both active and passive microwave systems have been found to have a linear response to soil moisture in the 15 to 30% range for given soil type. It has been shown that one must have information on the moisture/soil conditions in the top 30 cm of sediment to be of value in predicting trafficability conditions. However, the penetration sensing depth of microwave sensors is

limited to the top 2-5 cm of soil. There is, therefore, an obvious discrepancy between the requirement and present sensors.

AST, Inc. has initiated a soil moisture program using the laser/acoustic equipment described in this report. Initial measurements have demonstrated that it is possible to set up acoustic pulses in sand using the laser/acoustic techniques. Also, the characteristics of the acoustic signals appear to depend on the dryness of the sand. Continuing experiments are focused on establishing the relationship between the characteristics of the acoustic signals and the moisture content of the sand. We are also attempting to detect and isolate the acoustic signal in air (using a microphone) that is volume backscattered from the sediment. Although these initial measurements are encouraging, no definitive conclusions can be made at this time. A remote sensor system for sensing soil moisture based on the laser/acoustic technique could be extremely powerful.

4. References

Bell, C. E. and J. A. Landt, 1967. Appl. Phys. Letters 10, 46.

Brewer, R. G. and K. E. Rieckhoff, 1964. Phys. Rev. Letters 13, 334.

Bunkin, F. B., N. V. Karlov, V. M. Komissarov and G. P. Kuzmin, 1971. Zh ETF Pis. Red 13, 9, 479. (English translation: Sov. Phys. - JETP Letters 13, 341 (1971).

Carome, E. F., C. E. Moeller and N. A. Clark, 1966. JASA 40, 1462.

Cawley, R. G. and C. E. Bell, 1972. "Propagation of CO_2 Laser (10.6μ) Induced Pressure Transients in Water (U)," NOLTR-72-107, Confidential.

Edmonds, John A. and G. Daniel Hickman, 1981. "An Assessment of the Requirements and Techniques for Remote Sensing of Trafficability," Contract No. N66001-80-0106. Applied Science Technology, Inc Report AST-R-140981.

Hickman, G. D., Bernadette Johnson and Gail Ann Hickman, 1981. "Summary of Remote Sensing Techniques for Sensing Soil Moisture: Annotated Bibliography," Contract No. N66001-80-C-0106. Applied Science Technology, Inc. Report AST-R-120181.

Hickman, G. D., B. S. Maccabee and C. E. Bell, 1980. "Feasibility Study of Airborne Bathymetric Sensing Using the CO_2 Laser/Acoustic Technique," Contract No. N00014-78-C-0764. Applied Science Technology, Inc. Report AST-R-070580.

Hickman, G. D., 1975. "A New Concept for a Rapid Surveillance Acoustic Bathymetric System," N00014-71-C-0202, SPARCOM, Inc., Technical Report.

Lowney, J. R. and J. B. Sullivan, 1970. "Interaction of CO_2 Laser Radiation and Water," NOLTR 69-166 (Naval Ordnance Laboratory).

Maccabee, B. S. and C. E. Bell, 1977. "Properties of Laser Induced Sound in the Ocean (U)," Naval Surface Weapons Center, NSWC/WOL/TR (Confidential).

5. Relevant Conference Presentations

1. Laser-Induced Luminescence for Measurement of Nearsurface Temperature and Salinity and Laser/Acoustic Technique for Shallow Turbid Water Bathymetry. Presented at Bolkesjø Workshop on Remote Measurement of Underwater Parameters, Bolkesjø, Norway, October 30-November 1, 1980.

2. Airborne-Surface Acoustic Ranging Technique, Fifteenth International Symposium on Remote Sensing of Environment, Ann Arbor, Michigan, May 11-15, 1981.

3. A Laser-Generated Acoustic Remote Sensing Technique for Subsurface Ranging, Submitted for presentation at the International Symposium on Underwater Acoustics in Tel Aviv, Israel, June 15-18, 1981.

APPENDIX A

MICROPHONE REFLECTOR GEOMETRIES FOR LASER/ACOUSTIC BATHYMETRY

Overview

A laser/acoustic bathymetry technique has been described (Hickman, 1981) in which energy, deposited on the surface of water by a narrow, pulsed, infrared laser beam incident from above the air-water interface, gives rise to an acoustic pulse that propagates within the water medium. Some of the energy in this pulse can be redirected toward the interface by underwater objects, where additional reflection occurs. Most importantly, however, a small fraction of the energy associated with the object-reflected acoustic pulse arriving at the surface is transmitted through the interface and propagates within the air medium. A sufficiently sensitive microphone located above the surface, then, allows detection of this energy.

Preliminary experiments, enlisting a microphone with reflective optics fashioned from components at hand, have demonstrated the principle. It is the purpose of the effort reported on here to explore at some depth, detail of microphone reflector geometries with the view toward their optimization. Additionally, practical trade-offs between competing approaches are considered. Finally, a particular geometry is recommended for fabrication.

No account is given to constraints that, ultimately, may be imposed by operational mission considerations. Thus, for instance, relative mass, differing form-factors, etc., are not considered.

The analysis that follows borrows heavily from the theory of the simple microwave paraboloid antenna, the theory of Cassegrainian optics (used both at microwave and optical frequencies) and empirical microwave reflector data extant in the literature.

General Considerations

It is assumed that the microphone element to be used will be a B&K type 4149 Condenser Microphone. Using a microphone diameter of 1.27 cm and assuming a cylindrical piston microphone model, the angular response patterns have been calculated for frequencies of 20, 30, and 40 kilohertz, according to the relation (Kinsler, 1962):

$$I(\theta) = 20 \log \frac{2J_1((2\pi a/\lambda)\sin\theta)}{(2\pi a/\lambda)\sin\theta}, \qquad (1)$$

where: $I(\theta)$ is the microphone response at angle θ, in decibels, relative to response along its axis,

J_1 = the first order Bessel Function,

a = the radius of the microphone diaphram,

λ = the wavelength of sound in air,

θ = angle measured from the microphone axis.

Equation (1) is presented graphically in Fig. A1 along with observed responses for the B&K 4149 Condenser Microphone obtained from published data (B&K, 1980).

The agreement between calculated and published values is relatively good. Therefore, the angularly continuous response given by the "piston microphone" model will be used in the subsequent analysis. Out emphasis will be in optimizing the microphone's response at 30 kHz. For distinct reasons, performance will tend to degrade at frequencies that are either significantly higher or lower than 30 kHz.

The next question to be considered is that of dimension. In order that the potential gain of a given aperture be fully realized, the sound source (reflecting object) must be in the far-field of the aperture. This range condition is usually expressed (Kandoian, 1968):

$$S \geq \frac{2D^2}{\lambda} \qquad (2)$$

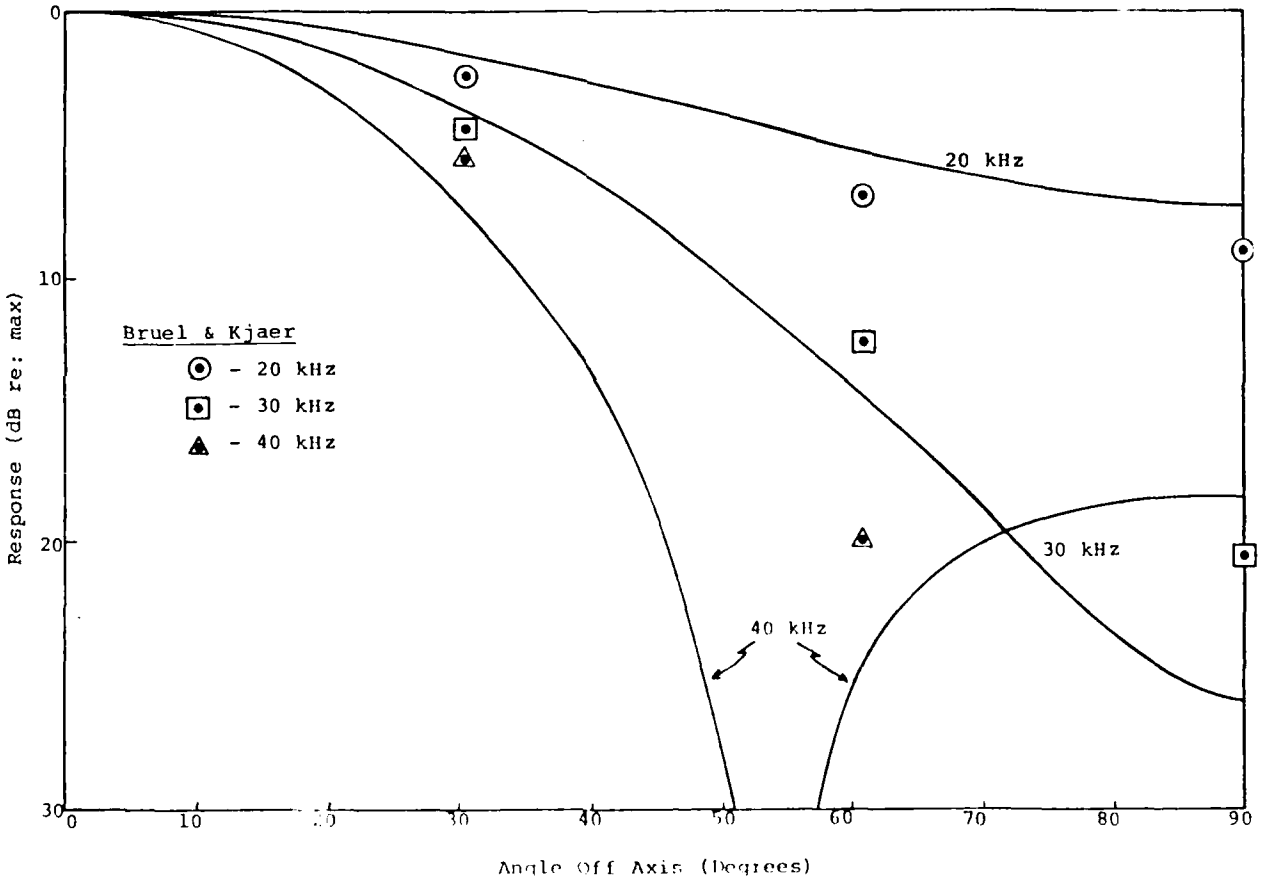

Figure A1: Angular Response of Microphone

where: S = source to aperture range,

D = diameter of aperture,

λ = wavelength of sound (in air).

Using this expression, we find in order to achieve maximum gain for a 35 cm diameter aperture at 30 kHz, in air, that the range to the source(s) must be at least 22 meters; this range condition increases to at least 45 meters for a 50 cm diameter aperture. Because of refraction of acoustic rays at the air/water interface, an underwater source will create a virtual image at a distance that is five times greater than the actual source distance. Assuming that the majority of the acoustic path is in water, the effective far field ranges will be about 4.5 and 9.0 meters respectively. Thus, it would appear that apertures as large as 0.5 meters would be practical.

If reflector tolerance is held to within $\pm$ 0.1 wavelengths, negligible directivity degradation will result. At 30 kHz, this corresponds to about $\pm$ 0.1 cm. This value will be assumed to apply throughout.

The Simple Parabolic Reflector

With microwave paraboloid antennas it has been found that theoretical aperture efficiencies as large as 80% can be achieved by correctly matching the directional characteristics of the feed and the geometry of the reflector. In practice, aperture efficiencies of 50-60% are attained. Greatest aperture efficiency results when the illumination at the edge of the paraboloid due to the feed is about 10 dB below the level of illumination at the apex (Kandoian, 1968). (Since the angular response and directivity of an antenna or an acoustic transducer is independent of whether or not it is used for transmitting or receiving, according to the principle of reciprocity, the analysis may be made for either a transmitter or receiver.) It is convenient, to use the parlance of the transmitting case that considers the feed as a radiating source. A feed with a narrower pattern, that is one that results in a

smaller edge illumination, will utilize the outer reflector area ineffectively; a broader feed pattern will cause "spill-over" and a significant fraction of the total radiated power will not be redirected by the reflector.

The illumination at a point on the reflector is not only dictated by the angular response of the feed but, also, it depends on the feed-to-reflector distance to that point. The feed-to-reflector range is derived, using the equation of a parabola in polar coordinates having a focus at the polar origin (Silver, 1949).

Thus:

$$L(\theta) = -20 \log (\sec^2 \frac{\theta}{2}), \qquad (3)$$

where: $L(\theta)$ = illumination level modification due to range, referred to the apex illumination level (dB),

θ = angle subtending the reflecting point and the paraboloid axis, at the focus.

The composite reflector illumination function obtained by combining the angular response of the microphone at 30 kHz (Figure 1) with the illumination level modification due to range given in Equation (3), is shown in Fig. A2. This graph shows that the composite -10 dB illumination level would occur at the edge of a paraboloid subtending $\pm 45^0$ at its focus. This angle, in turn, uniquely characterizes the focal length to aperture diameter ratio (F-number) of an optimum reflector. The relationship between these quantities is shown graphically in Fig. A3. The mathematical development of this expression is given in Silver, 1949. Thus, for a simple parabolic reflector, the optimum F-number will be 0.60 for the assumed microphone feed. A focal length of 21.0 cm is required for an aperture diameter of 35 cm, while a focal length of 30.0 cm is required for an aperture diameter of 50.0 cm.

The rectangular coordinates for generating the parabolas for each of these two apertures are tabulated in Table A1 along with the coordinates corresponding to spherical mirrors having the same focal length. (The expressions used in generating

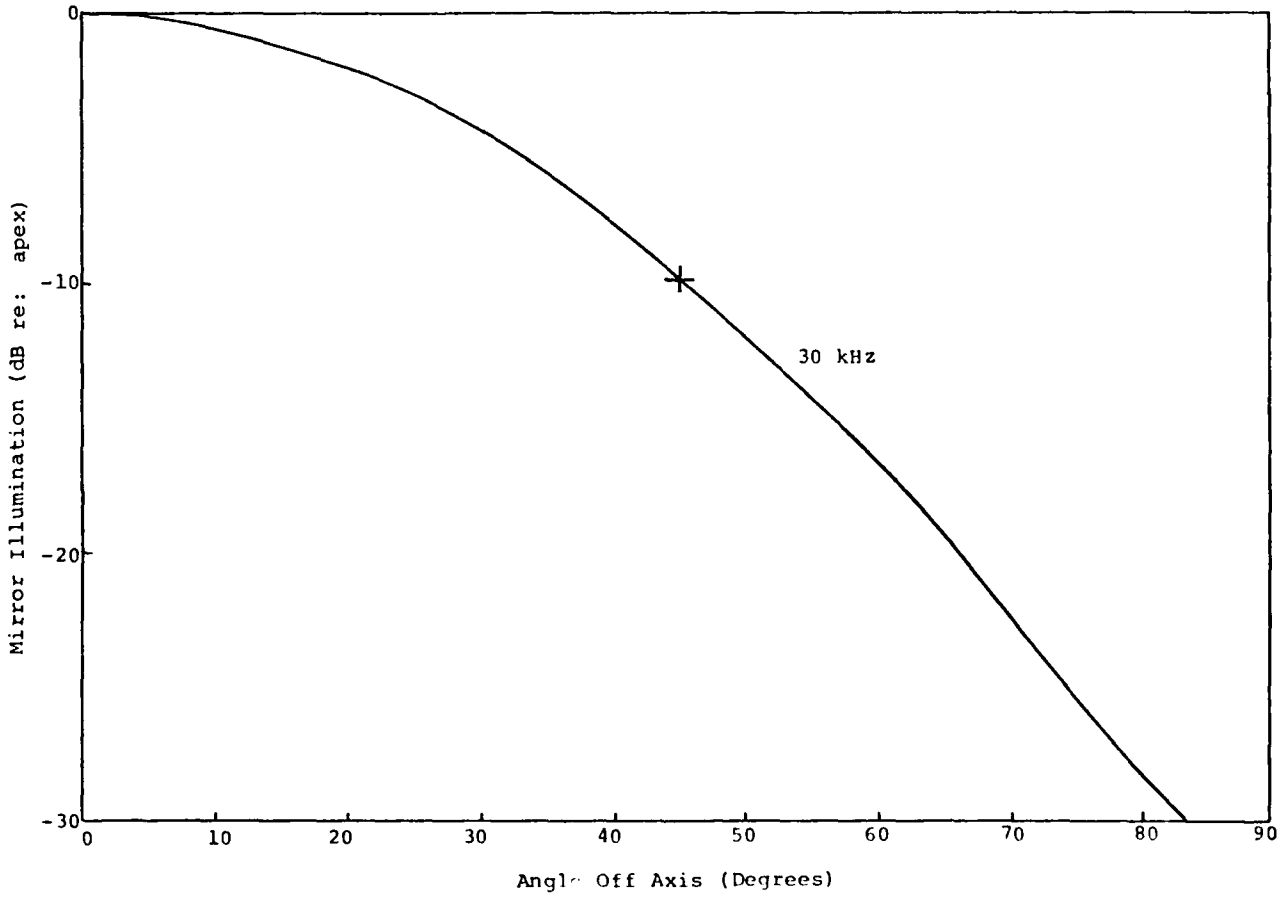

Figure A2: Paraboloid Illumination Function

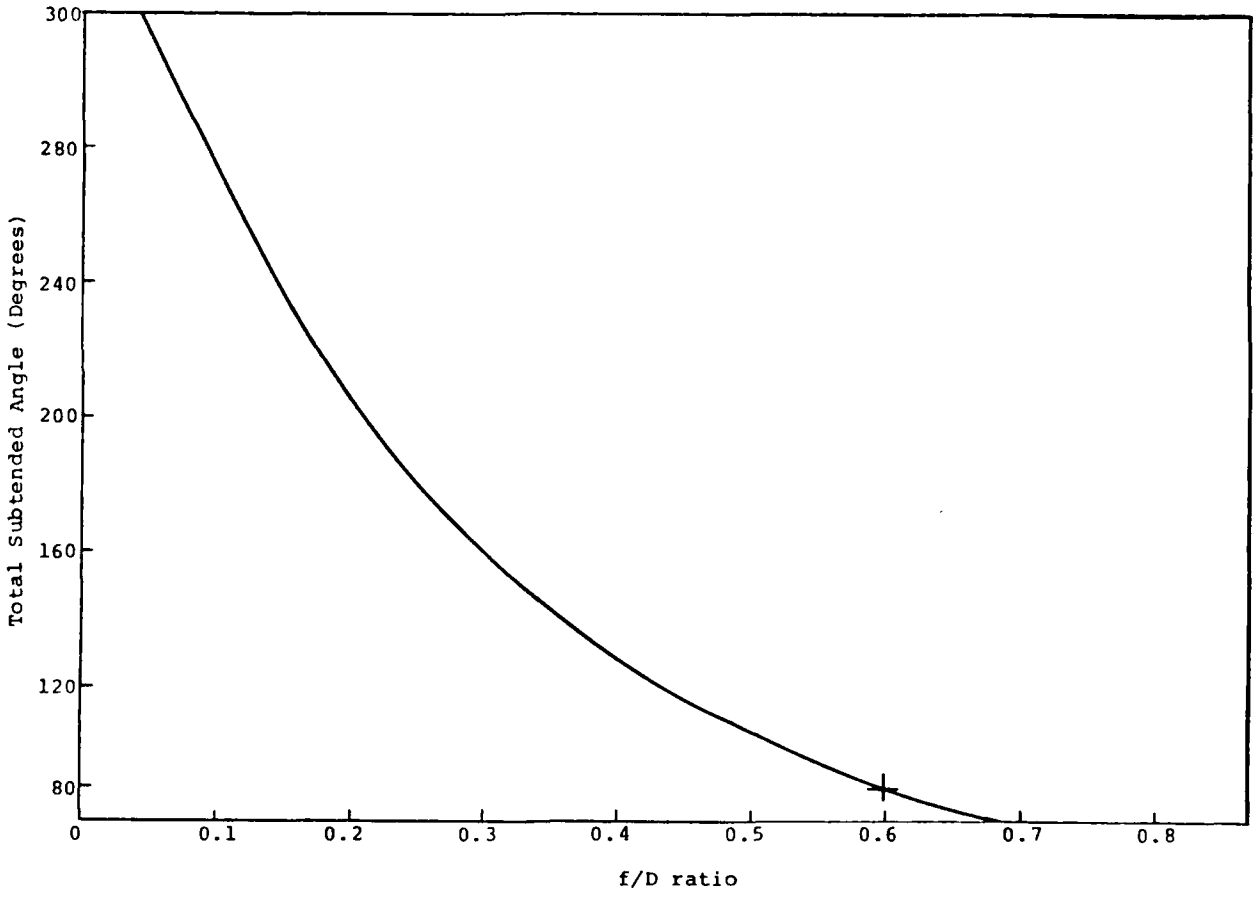

Figure A3: Angle Subtanded at Feed as a Function of f/D of Reflector

Diameter = 35.0 cm Focal Length = 21 cm			Diameter = 50 cm Focal Length = 30 cm		
X cm	Y Parabolic Reflector (cm)	Y Spherical Reflector (cm)	X cm	Y Parabolic Reflector (cm)	Y Spherical Reflector (cm)
0	0.00	0.00	0	0.00	0.00
1	0.01	0.01	1	0.01	0.01
2	0.05	0.05	2	0.03	0.03
3	0.11	0.11	3	0.08	0.08
4	0.19	0.19	4	0.13	0.13
5	0.30	0.30	5	0.21	0.21
6	0.43	0.43	6	0.30	0.30
7	0.58	0.59	7	0.41	0.41
8	0.76	0.77	8	0.53	0.54
9	0.96	0.98	9	0.68	0.68
10	1.19	1.21	10	0.83	0.84
11	1.44	1.47	11	1.01	1.02
12	1.71	1.75	12	1.20	1.21
13	2.01	2.06	13	1.41	1.43
14	2.33	2.40	14	1.63	1.66
15	2.68	2.77	15	1.88	1.91
16	3.05	3.17	16	2.13	2.17
17	3.44	3.59	17	2.41	2.46
17.5	3.65	3.82	18	2.70	2.76
			19	3.01	3.09
			20	3.33	3.43
			21	3.68	3.80
			22	4.03	4.18
			23	4.41	4.58
			24	4.80	5.01
			25	5.21	5.46

Table A1: Coordinates of Parabolic and Spherical Reflectors Having F Numbers of 0.6

these values are derived on page A-18.) It is apparent that the maximum divergence between the parabolic and spherical reflector figure approaches $\frac{\lambda}{4}$ at 30 kHz so that a significant directivity penalty could be expected if the reflector figure were spherical rather than parabolic. Off-axis aberrations are ignored; it is presumed that the aperture axis is properly aligned with the source.

The effective areas of the apertures under discussion can be obtained from the relation:

$$A_{eff} = q(\pi r^2), \tag{4}$$

where: A_{eff} = effective area,
q = aperture efficiency (assumed = 0.55)(Kandoian, 1968),
r = reflector aperture radius.

The directivities that can be attained by these apertures can be derived according to the expression (Kandoian, 1968):

$$D(dBi) = 10 \log (4\pi A_{eff}/\lambda^2) \tag{5}$$

The resulting values of effective areas and predicted practical directivities are shown in Table A2. The gain enhancement brought about by the reflector, (referenced to the microphone without reflector) is also given.

	APERTURE	
	35 cm	50 cm
Effective Area (Cm^2)	529	1080
Directivity (D)--dBi	37.4	40.5
Gain Over Microphone Alone--dB	24.6	27.7

Table A2: Reflector Effective Areas and Directivities

In the determination of the Gain over Microphone alone, the microphone directivity was determined through the use of Fig. 1 and,

$$D_m = 10 \log(2/(1 - \cos \theta/2)) \quad (6)$$

where: D_m = the microphone directivity (dBi)
θ = the equivalent beamwidth (3 dB).

This expression results in a microphone-only directivity of 12.8 dBi. Subtracting this quantity from the aperture directivity yields the directivity enhancement of the reflector.

The effective areas given in Table 2 are useful for estimating the actual acoustic power (Watts) delivered to the microphone, for an aperture-incident plane wave having a specified rms pressure amplitude (Kinsler, 1962).

Thus:

$$P = \frac{p^2}{\rho c} A_{eff} \quad (7)$$

where: P = the power delivered to the microphone (Watts)
p = the rms pressure amplitude (Pascals)
ρc = the acoustic impedance of air in Rayls (415; $\rho = 1.21$ kg/m^3, $c = 343$ m/s)
A_{eff} = the effective area (m^2)

Cassegrain Reflectors

The Cassegrainian optical system is inappropriate in the regeme of interest. Secondary, as well as primary, reflectors must be large in terms of wavelength so that ray optics can be applied. Simultaneously, secondary mirrors must be kept small with respect to the primary mirrors in order to minimize aperture blockage and preserve directivity. Imposition of these simultaneous requirements implies the need for primary apertures that are much larger than a wavelength. (Typically, with microwave Cassegrainian systems, the primary reflector is hundreds of wavelengths in diameter; with optical telescopes it is far larger.) In the acoustic case of interest (30 kHz),

the primary reflector will be less than 100 wavelengths in aperture and the secondary reflector will be, at most, only several wavelengths in diameter.

Some approximate designs will be considered, however, with the caveat that appreciable deviation from calculated performance based on the primary reflector aperture could be expected, as the consequence of the failure of the ray-optic approximation.

The use of the secondary reflector in the Cassegrainian geometry as shown in Fig. A4. permits the system focal length (and hence focal length to aperture ratio) to be increased beyond that characterizing the primary mirror alone. The secondary reflector can be regarded as a matching device allowing optimum performance to be attained for a given combination of primary reflector and feed.

The initial laser/acoustic bathymetry experiments employed Cassegrainian optics using reflecting surfaces that were easily obtained. The primary mirror had a diameter of 35.2 cm, and the microphone was inserted through a hole in the back of the mirror. Radii of curvature measured with a standard tripod spherometer are given in Table A3.

Location	Radius of Curvature (cm)	Standard Deviation (cm) (5 Measurements)
near central perforation	22.02	2.37
midway to edge	25.42	3.19
near edge	25.76	2.83

Table A3: Measured Radii of Curvature of Primary Mirror

From the radii measurements, it would appear that the mirror is aspheric and, possibly, could be parabolic. The large fractional standard deviation characterizing the measurements could be due, in part, to the interaction of the compound curvature of the surface of a paraboloid and the random angular orientation

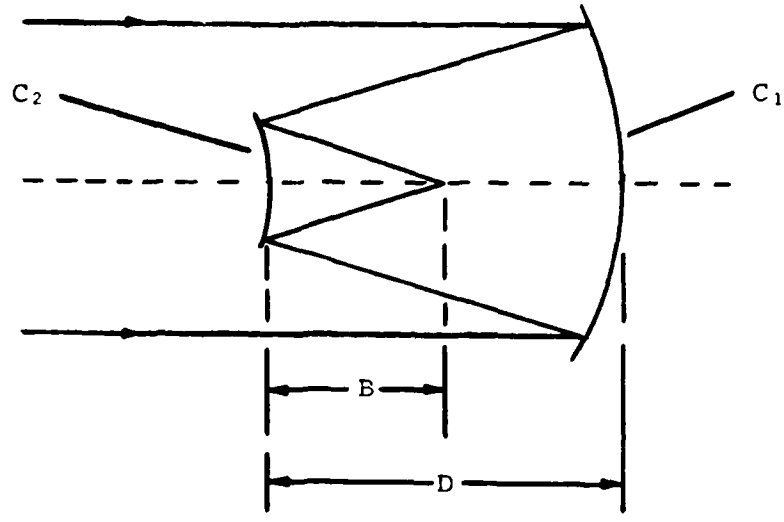

C_1 = curvature of primary reflector (reciprocal of radius of curvature)

C_2 = curvature of secondary reflector

f = system focal length

B = distance from secondary to back focus

D = distance between mirrors

Figure A4: Cassegrainian Optical System

of the spherometer tripod legs. (Expressions for the radii of curvature of a paraboloid in the meridianal plane (plane containing a generating parabolic) as well as in the orthogonal plane are derived on page A-19. Numerical values have been tabulated there for a paraboloid having a near-apex radius of curvature of 22 cm (Focal Length = 11 cm).

The secondary mirror used in the initial experiments appears spherical, having a radius of curvature of 4.26 cm. The standard deviation of the measurements was 0.27 cm (5 observations).

If this primary mirror is to be used in a future system, it will be imperative that its focal length be better defined, possibly by means of a lens gauge (a device similar to the spherometer but having a pair of fixed legs, each uniformly distant from and on opposite sides of an adjustable central probe; instead of the tripod legs of the spherometer). This allows the radii of curvature in orthogonal planes to be measured independently.

For the purpose of the approximate designs, it is assumed that this reflector is parabolic with a radius of curvature at the apex of 21.76 cm (derived from measurements made closest to central hole). Thus, its focal length to aperture ratio is taken to be 0.31, a value that is much less than that required for optimal matching the microphone to the receiver in a single reflector system.

The preliminary design equations for a Cassegrainian system are (Driscoll, 1978):

$$C_1 = \frac{B-f}{2Df}, \tag{8}$$

and,

$$C_2 = \frac{B+D-f}{2BD}, \tag{9}$$

where the symbols have their meanings assigned to them in Fig.4. Given B, D and f, a fourth order "aspheric deformation coefficient" can be obtained for the secondary mirror. This coefficient together with its apex curvature, C_2, defines its

shape. If the primary mirror has a parabolic figure (as assumed), the deformation will result in a hyperboloidal secondary reflector (classic Cassegrain). On the other hand, should the primary mirror be spherical, the shape of the secondary will not be as simple. In either case, however, the effects of spherical aberration can be suppressed.

Possible Cassegrainian System Making Use of Present Primary and Secondary Optical Reflectors

In this design, we accept the present optical elements and stipulate a value for system focal length. In this case, C_1, C_2 and f are given and the initial problem is to determine the distances B and C. Combining equations (8) and (9) yields:

$$B = \frac{fC_1+0.5}{C_2} \tag{10}$$

$$D = \frac{f(C_1-C_2)+0.5}{2fC_1C_2} \tag{11}$$

using $C_1 = -\frac{1}{21.76}$, $C_2 = -\frac{1}{4.26}$, f = 19.20. Calculations yield an F number of 0.55, B = 1.63 cm and D = 9.96 cm.

This design can be rejected immediately because of the extreme proximity of the microphone to the secondary mirror ($\simeq$ 1 wavelength).

Possible Cassegrainian Systems Making Use of Present Primary Reflector

In these designs only C_1 and f are specified and the independent variables are C_2, B and D. Equations (8) and (9) thus allow freedom for one additional constraint to be imposed.

B = D Constraint. A convenient geometry may result if B is set equal to D. With this additional condition, equations (8) and (9) yield:

$$B = D = \frac{f}{1-2fC_1}, \tag{12}$$

$$C_2 = \frac{2(1-2fC_1) - (1-2fC_1)^2}{2f}. \tag{13}$$

Taking the values for C_1 and f as before, yields a value for C_2 of 0.055 cm^{-1}. The secondary radius of curvature is calculated to be -18.16 cm and B = D = 6.94 cm.

Knowing B, D and f and assuming the primary reflector is paraboloid, the equation of the secondary mirror that cancels on-axis aberration can be derived from the fourth order "aspheric deformation coefficient" (K_2) and the required value of C_2 itself. The value of K_2 is given by (Driscoll, 1978):

$$K_2 = \frac{(f-D-B)(f+D-B)^2}{64\ B^3} \qquad (14)$$

so that, in this case, $K_2 = 2.743 \times 10^{-4}\ cm^{-3}$ and the equation for the convex secondary mirror is

$$Y(cm) = R_2 - \left\{R_2^2 - X^2\right\}^{\frac{1}{2}} - K_2X^4 \qquad (15)$$

or;

$$Y(cm) = 18.16 - \left\{18.16^2 - X^2\right\}^{\frac{1}{2}} - 2.743X10^{-4}X^4 \qquad (16)$$

Values of Y (equation 16) are given for this secondary mirror in Table A4.

X (cm)	Y (cm)
0	0
1	-0.03
2	-0.11
3	-0.23
4	-0.38
5	-0.53
6	-0.66
Note: Y taken as negative to correspond to upward facing convex surface	

Table A4. Coordinates for Secondary Mirror, Given B = D

B = D/2 Constraint. Using the same numerical values that were used previously for f and C_1, it follows that C_2=-0.09 cm^{-1} (radius of curvature -11.09 cm), B=4.24 cm and D=8.48 cm. From equation (14), K_2 is calculated to be 1.197 x 10^{-3} cm^{-3}. The equation of the surface from equation (15) now becomes:

$$Y = 11.09 - \left\{11.09^2 - X^2\right\}^{\frac{1}{2}} - 1.197X10^{-3}X^4 \qquad (19)$$

Numerical values for the surface coordinates are given in Table A5.

In this case, a secondary mirror of about 8 cm diameter would seem to result in a good balance between secondary "spill-over" and loss due to obstruction.

X (cm)	Y (cm)
0	0
1	-0.04
2	-0.16
3	-0.32
4	-0.44

Table A5. Coordinates for Secondary Mirror, Given B = D/2

This last case represents a compromise in which the effective secondary aperture is neither intolerably small (as it would be in the case described on page A-14, as a consequence of feed proximity) nor unacceptably large (as in the case where B = D because of the resulting aperture blockage).

Conclusions and Recommendations

- In general, Cassegrainian reflectors are not well suited to the present task, primarily because of the conflicting requirements of the need for a large secondary aperture (in terms of wavelengths) and the need to restrict the dimensions of the secondary reflector to a small fraction of the primary aperture.
- The optical elements used in the initial experiment cannot be reconfigured to be effective.
- The Cassegrainian system of the original experiment could be improved somewhat by replacing the secondary reflector and positioning it as described on page 16. Performance would be poorer than the equivalent aperture used in a single reflector system, however, and cannot accurately be predicted without recourse to more rigorous analysis.
- The geometry that is recommended, and the one that represents the least risk and is the most amendable to reliable prediction, is the simple, single parabolic reflector. Such a reflector with a focal length to diameter ratio of 0.60 is matched to the B&K microphone and should yield a gain (relative to the B&K microphone response without reflector) of 27.7 dB for a 50 cm aperture or a gain of 24.6 dB for a 35 cm aperture.

Supplimentary Equations and Calculations

Spherometer Geometry

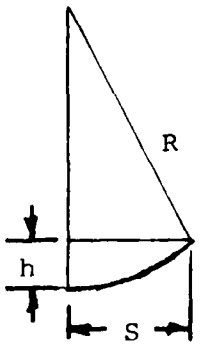

$$R^2 = S^2 + (R-h)^2$$

$$\boxed{R = \frac{h^2+S^2}{2h}}$$

Equation of Parabola with Apex at Origin

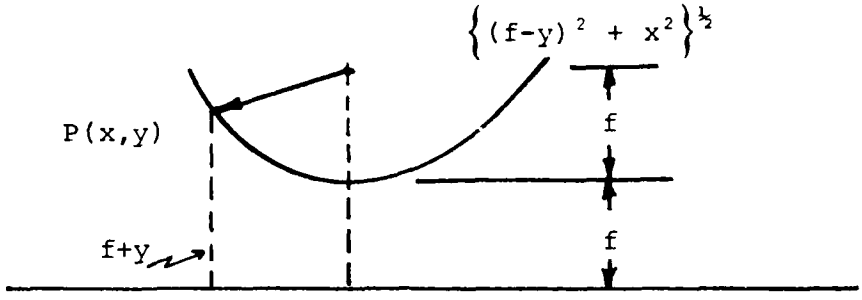

$$f+y = \left\{(f-y)^2 + x^2\right\}^{1/2}$$

$$\boxed{y = \frac{x^2}{4f}}$$

Radius of Curvature of a Parabolic Arc

The general expression for curvature of a parabolic arc in Cartesian coordinates is:

$$R = \frac{1}{K} = \frac{\left\{1 - (y')^2\right\}^{3/2}}{y''}$$

For a parabola with its origin at the apex:

$$y = \frac{x^2}{4f} \qquad y' = \frac{x}{2f} \qquad y'' = \frac{1}{2f}$$

so that:

$$\boxed{R = \left\{2f(1-\tfrac{1}{4}(\tfrac{x}{f})^2)\right\}^{3/2}}$$

This also corresponds to the radius of curvature of a paraboloidal surface in the meridianal plane.

Radius of Curvature of a Paraboloid in Plane Normal to the Meridianal Plane

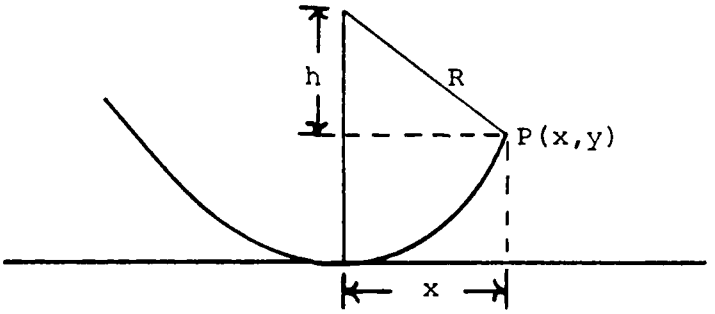

The slope of the parabola at P (x, y) is given by

$$y' = \frac{x}{2f},$$

while the slope of the normal to the parabola at P (x, y) is

$$-\frac{1}{y'} = -\frac{2f}{x},$$

so that:

$$h = -x\left(-\frac{2f}{x}\right) = 2f,$$

and:

$$R = \left\{x^2 + 4f^2\right\}^{\frac{1}{2}}.$$

The radii of curvature of a paraboloid having its apex radius of curvature corresponding to that measurement for the original reflector are calculated in Table A6 below.

Distance from Apex (cm) (X)	Radius of Curvature (cm) Meridianal Plane	Orthogonal Plane
0	21.76	21.76
2	22.04	21.85
4	22.87	22.12
6	24.29	22.57
8	26.32	23.18
10	29.01	23.95
12	32.41	24.85
14	36.59	25.87
16	41.61	27.01
18	47.56	28.24

Table A6: Calculations for Parabolic Reflector

Equation of a Circular Arc Having Radius R and Focal Length f with Its Origin at Apex

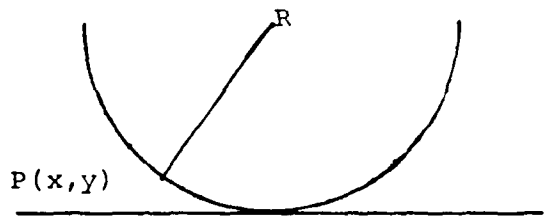

$$(R-y)^2 + x^2 = R^2$$

$$\boxed{y = R \pm \left\{R^2 - x^2\right\}^{\frac{1}{2}}}$$

Note: The negative sign before bracketed quantity is taken for upward concave surface as shown in sketch.

since R = 2f:

$$\boxed{y = 2f - \left\{4f^2 - x^2\right\}^{\frac{1}{2}}}$$

Angle Subtended at Focus of Parabola vs. Focal Length to Aperture Ratio

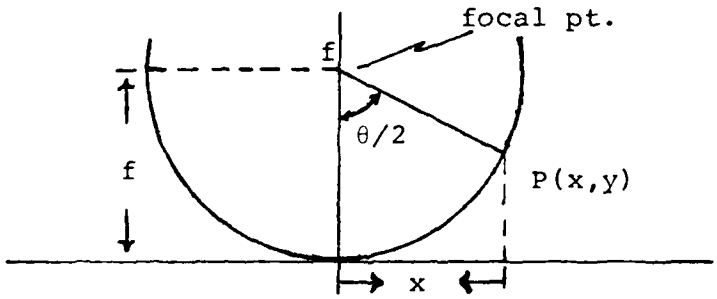

$$\tan\frac{\theta}{2} = \frac{x}{f-y} = \frac{x}{f-\frac{x^2}{4f}} = \frac{4fx}{4f^2-x^2}$$

but the focal length to aperture ratio is:

$$F = \frac{f}{2x}$$

so that

$$\tan\frac{\theta}{2} = \frac{8F}{16F^2-1}$$

or

$$\boxed{\theta = 2\tan^{-1}\left\{\frac{8F}{16F^2-1}\right\}}$$

REFERENCES

Brodhage, H. and W. Hormuth. Planning and Engineering of Radio Relay Links, Siemens, 1977.

Bruel and Kraer Instruments, Master Catalog, 1980

Conrady, A. Applied Optics and Optical Design, Oxford University Press, 1929; Dover, 1957.

Driscoll, W. Handbook of Optics, Optical Society of America, McGraw-Hill, 1978.

Hickman, G. D., J. S. Bailey and B. S. Maccabee. "Airborne-Surface Acoustic Ranging Technique", Fifteenth International Symposium on Remote Sensing of Environment, Ann Arbor, Michigan, May 1981.

Kandoian, A. Reference Data for Radio Engineers, 5th Edition, ITT, 1968.

Kinsler, L. and A. Frey. Fundamentals of Acoustics, Second Edition, Wiley, 1962.

Silver, S. Microwave Antenna Theory and Design, MIT, Radiation Lab Series, Volume 12, 1949, also Dover.

Skolnik, M. Introduction to Radar Systems, McGraw-Hill, 1962.

APPENDIX B

POSSIBLE MEANS FOR ENHANCING THE SENSITIVITY OF THE LASER/ACOUSTIC BATHYMETRY SYSTEM

Considerations Regarding System Sensitivity and Directivity

A previous report (Green, 1981) showed that microphone directivities as large as ≈ 28 dB can be attained at 30 kHz with paraboloid reflectors of practical size (diameter = 0.5 meters). This directivity derives, of course, from the constriction of beamwidth achieved by such an aperture.

Due to refraction at the water-air interface, sound of subsurface origin will appear, to an observer in air, to originate within a cone of 26.4° centered on the nadir (assuming a plane and horizontal water surface). A microphone providing this beamwidth could be considered "matched" to this arrival cone. Such a microphone would have a directivity of ≈ 18.5 dB. For microphones with greater directivity only a portion of the cone describing all possible arrival directions would be viewed. Some means should be provided, then, for guaranteeing detection over all angles. Depending on the velocity with which the microphone is moved in the operational situation and on the pulse repetition rate, it may not be necessary to cover the entire azimuth, however, only in directions nearly transverse to the microphone motion. It is necessary to obtain the greatest attainable microphone directivities in order to assure adequate signal to noise ratios. Therefore, the problem cannot be evaded by limiting directivity to the critical value without incurring a concomitant sensitivity degradation.

Surveillance by means of a sequentially scanned beam (produced either by mechanical motion or by an electronically scanned, phased array) would be precluded by the nature of the mission. At low angular scanning rates the acoustic return could be "missed" should the microphone be "looking" in the

wrong direction at the moment of its arrival. If, on the other hand, sufficiently rapid scanning rates were to be employed so as to insure that the beam would be swept over the entire potential arrival cone within the duration of the pulse, inordinately wide processing bandwidths would be required that would damage the signal to noise ratio. (Rather than the required bandwidth approximating the reciprocal of the pulse duration, it must be increased by a factor equal to the ratio of the solid angle of the potential arrival cone to the solid angle of the scanning beam; i.e., increased by the number of independent angular cells into which the arrival cone is resolved.) A solution to this dilemma would be to produce a cluster of simultaneous, narrow, overlapping beams that, together, would include the entire arrival cone.

Alternative Means for Generating Simultaneous Overlapping Beams

In principle, the entire beam set could be produced by: a multiplicity of properly directed large apertures, each with its own individual feed (microphone); a single large aperture reflector with a multiplicity of feeds on the focal surface; a single large aperture acoustic Luneburg lens with a multiplicity of feeds, or; a multielement array disposed over a single large aperture from which the required beam set could be synthesized.

Multiple Apertures

The first of these approaches would seem unlikely to offer a practical solution because of weight and space limitations imposed by the mission.

Single Reflecting Aperture--Multiple Feeds

While the second alternative cannot be dismissed summarily, formidable difficulties would be ancountered in the placement of the required cluster of feeds (microphones), consequent aperture blockage and off-axis reflector aberrations. (Multiple-feed, common-reflector antennas are used with microwaves for

multibeam generation in "monopulse" radar applications.) However, such designs usually are limited to the production of few beams and have apertures that are greater in terms of wave-lengths than has the acoustic aperture of our interest.

Single Refracting Aperture (Luneburg Lens)--Multiple Feeds

The problems of feed placement, aperture blockage and off-axis aberrations could be avoided entirely, through the use of an acoustic Luneburg lens, rather than reflecting "optics." Such a lens, depicted in Fig.B1, is spherical in form and has an acoustic propagation velocity that is described by the relation:

$$c(r) = c_o \left\{ 2 - \left(\frac{r}{R}\right)^2 \right\}^{-\frac{1}{2}}, \qquad (1)$$

where: $c(r)$ = the propagation velocity at radius r
c_o = the propagation velocity at the surface
r = the radius of the lens

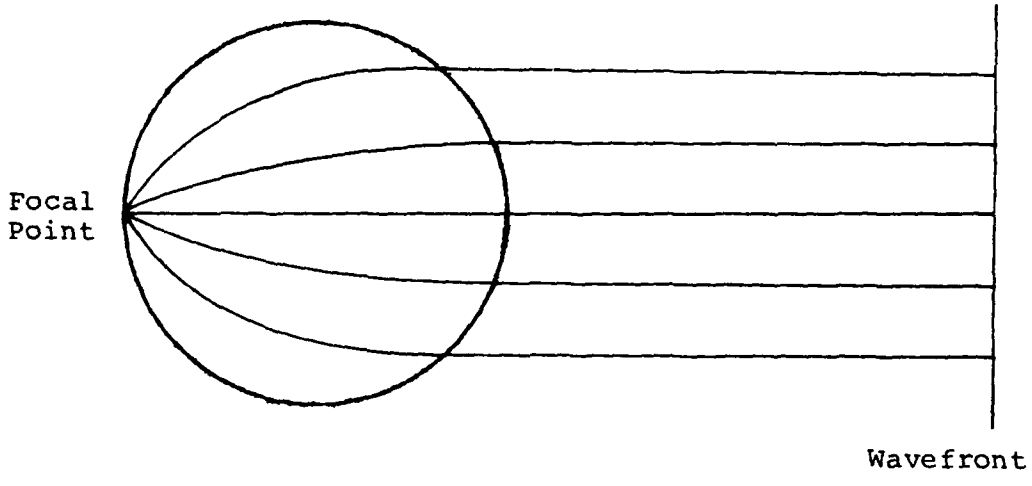

Luneburg Lens

Fig. B1

It has been shown (Luneburg, 1964) that such a refracting structure has the property of focussing an incident plane wave to a spot (diffraction limited by aperture size) on the surface of the sphere that is diametrically opposite to the direction of incidence. Since the feed and the effective aperture are on opposite sides of the sphere, there is no aperture blockage. Because the focal surface has a large radius of curvature, that of the lens itself, there is no conflict in multiple feed placement. (In contrast, the focal surface associated with the reflector of the second alternative would be highly curved.) Since the lens has spherical symmetry, there are no off-axis aberrations and the entire arrival cone could be accommodated by distributing feeds (microphones) over a spherical cap of 26.4°.

Despite the elegance of this approach, its practical attainment may be thwarted by difficulties encountered in the fabrication of the required acoustically inhomogenous lens. Ideally, the lens would: 1) have the largest aperture that space constraints would permit ($\approx$ 0.5 meters); 2) have an acoustic impedance at its surface close to that of air to prevent reflection at the air-lens interface (and consequent resonances); 3) possess an internal velocity profile described by equation (1); and 4) be nearly lossless in the vicinity of 30 kHz. These characteristics, particularly the second, suggest that the lens material must be principally gaseous.

An abbreviated survey of the literature has disclosed successful operation of acoustic Luneburg lenses for underwater applications by various worders (Boyles, 1977; Byron, 1974), but no references to lenses designed to operate in air were uncovered. It is well known that practical Luneburg lenses for microwaves have been fabricated with artificial dielectrics. (Elliott, 1981)

Simultaneous Multibeam Phased Array

In this alternative, n microphone elements of relatively low directivity are disposed over an aperture surface (probably

plane surface). The output from each element is independently amplified and divided m ways, where m is the number of simultaneous beams that are formed. Amplification is necessary in order that the power division operation does not reduce system sensitivity significantly. (The element amplifiers must have a low noise figure and sufficient gain so that a low overall system noise figure is established at their output, despite subsequent power division and post amplifier noise contributions.) Each of the m beams is synthesized by taking one of the divided outputs from each element amplifier, interposing a proper time delay and combining the delayed outputs. (It should be noted that, although this array is truly a phased array, the large fractional bandwidth involved prevents the use of narrow band phase shifters.) True time delays are required to compensate for the differences in arrival time of the wave front at the individual elements. Figure B2 attempts to illustrate this beam-forming arrangement.

A design strategy requiring the least number of array elements (and attendant signal handling/processing components) would select elements that are "matched" to the 26.4° potential arrival cone. Such an element would have an aperture of $\simeq 0.04$ meters and could be constructed with a wide angle feed (microphone) and a parabolic reflector of this diameter. The array ensemble, then, would comprise a single plane surface in which parabolic depressions are formed together with the associated feeds. Figure B3 demonstrates this concept. Alternatively, simple refractive acoustic lenses of this same aperture might be used instead of the reflectors. Figure B4 shows typical beams that might be synthesized with such a minimum element array. As frequency varies over the 20-40 kHz band, the angular orientation of the beam maxima will remain fixed. Beamwidths will vary inversely with frequency.

Depending on the microphone translation velocity and the pulse repitition rate, it may be possible to limit surveillance to azimuths close to the direction that is transverse to the

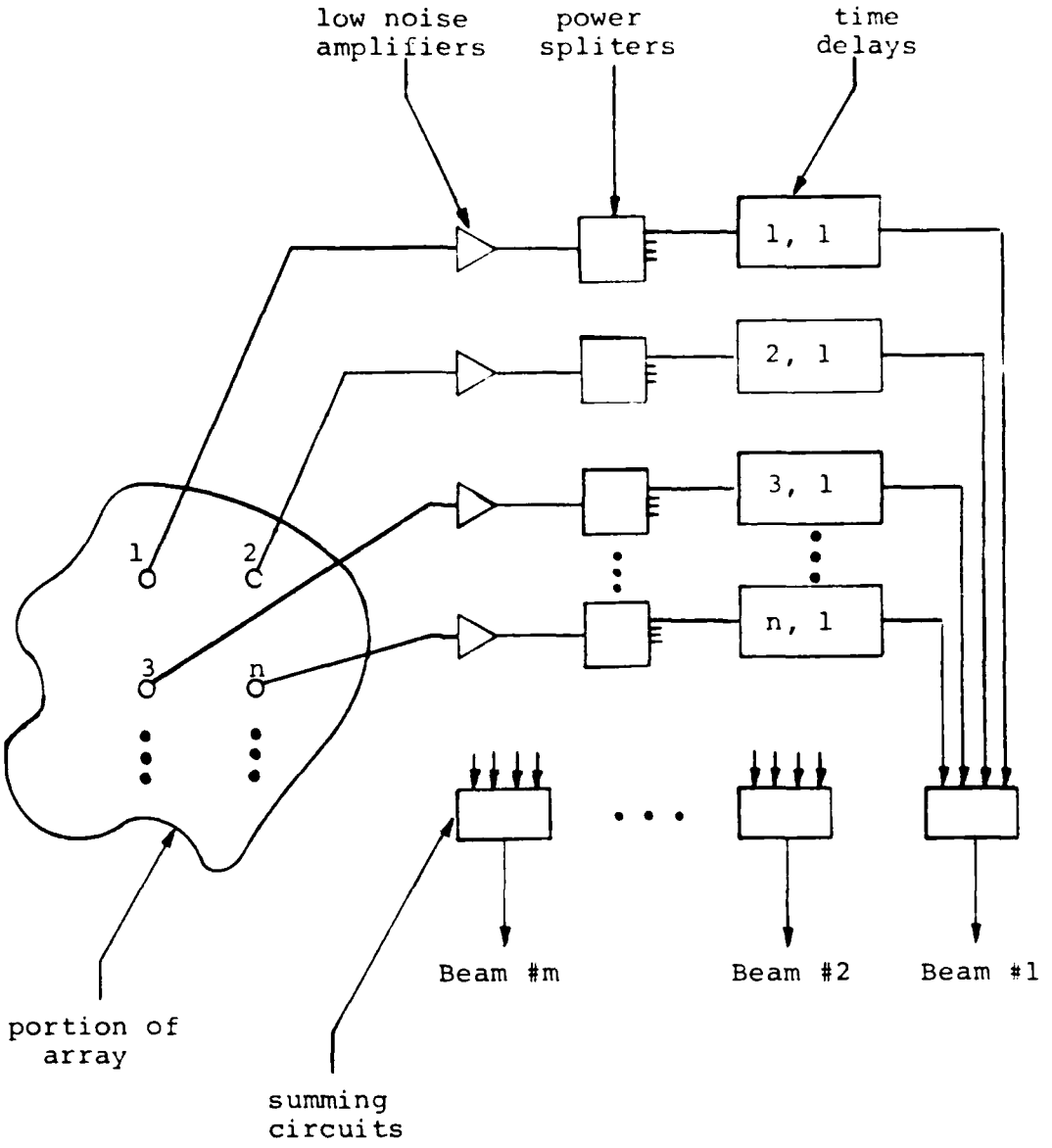

Simultaneous Beam Forming Network

Fig. B2

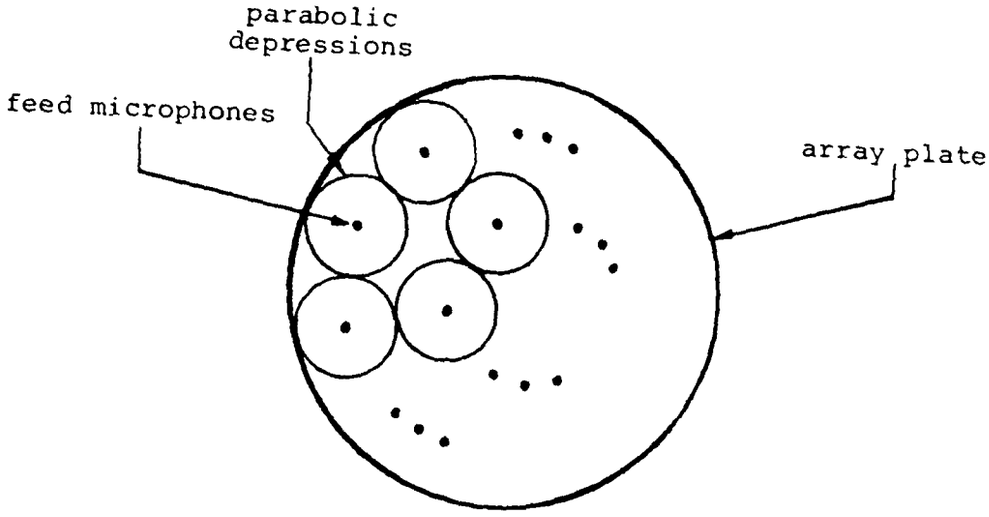

Mosaic of Parabolic Reflector Microphones

Fig. B3

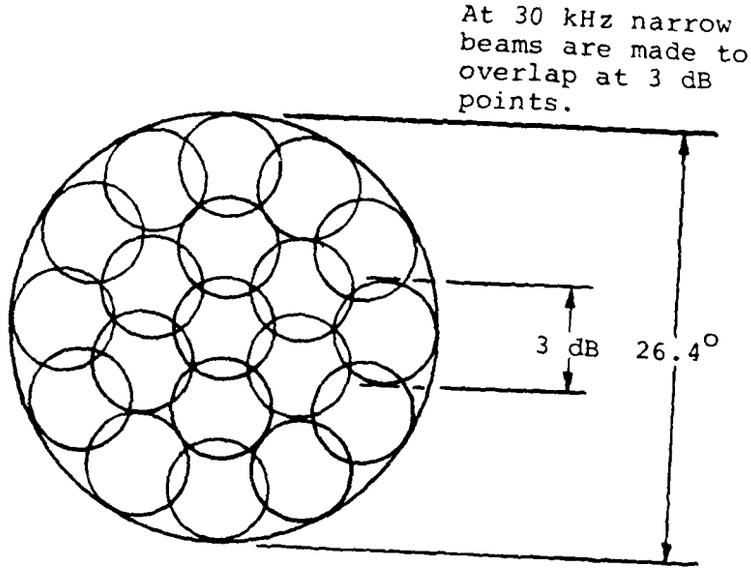

Simultaneous Beam "Foot Print"

Fig. B4

microphone motion. In this circumstance linear, rather than two-dimensional arrays could be employed. The axis of the array would be in the direction of motion and it would be used to produce a set of narrow "fan" beams in the vicinity of its normal, much as is the case with underwater "towed arrays." This practice would simplify the beam-forming networks.

The necessary time delays for beam generation could be implimented with acoustic delay lines (frequency translation might be required to match the operating frequencies of commercially available delay lines), analog charge coupled devices (CCD), or with analog tape loops or magnetic discs. For an array having an aperture of 0.5 meters, maximum delays required in the beam forming networks would be ≈ 335 microseconds.

Multibeam synthesis also could be accomplished digitally. In this case, the signal from each element, after amplification, would be digitized at a rate sufficient to satisfy the Nyquist requirement and all of the necessary time shifting and combining operations would be accomplished in parallel digital channels. This would obviate the need for any of the hardware described above. The choice of which of these courses to follow depends on the relative costs, sizes, weights and power requirements involved.

Microphone Efficiency--Gain

It has been implicitly assumed that the microphone (feed) is perfectly efficient; i.e., the directivity and gain are equal. (Gain = Efficiency x Directivity.) A reduction of efficiency produces a corresponding diminution in gain and a deterioration of system sensitivity. (Reduced efficiency is harmful in two ways: less signal related power is available to compete with noise originating in the following amplifier, and; thermal noise associated with the loss resistance is added.)

It appears that the B&K microphone presently used is purposely damped through the introduction of mechanical loss

to prevent gain increase with frequency that otherwise would be expected. In this way the microphone response is kept "flat", a desirable attribute in many circumstances when the ultimate high frequency sensitivity is not needed and the dynamic range of subsequent electronics is limited. In the application at hand, however, the complete elimination of this loss in the 20-40 kHz interval would correspond to increasing the aperture diameter by a factor of ≈ 3.

Summary and Recommendations

Array

If microphone directivities less than 18.5 dBi can result in an adequately sensitive system, then a single, simple parabolic reflecting aperture will suffice for surveillance.

- A preliminary array geometry should be designed and its performance estimated.
- A trade-off analysis should be made between the various alternative methods of accomplishing the delay and combining operations necessary for array beam synthesis.

Luneburg Lens

If, as is likely, greater directivities than 18.5 dBi are required, simultaneous overlapping, narrow beams must be formed. This might be accomplished through the use of a Luneburg lens. (This approach must be considered a "long shot" because of potential difficulties in lens fabrications but potential "payoff" is large in terms of system simplicity.) More conventionally, the beams could be formed with an array of relatively low directivity elements. A particularly advantageous configuration would enlist elements "matched" to the 26.4^{o} cone of potential acoustic arrival.

- A more complete library survey should be undertaken to uncover possible past efforts involving acoustic Luneburg lenses designed for use in air.
- Potential approaches for implementing such a lens should be identified.

Microphone Sensitivity

The present (microphone) feed appears to have a purposefully spoiled efficiency at the higher frequencies to offset the higher directivity at 0^{o} free-field incidence at these frequencies and result in a nearly frequency independent gain. System sensitivity would be greatly improved if the introduced loss could be removed.

- The manufacturer of the presently used microphone should be contacted to see if microphone efficiency in the 20-40 kHz region can be improved (at the expense of gain "flatness", of course). Of particular interest in this regard are the ½" and ¼" diameter microphones.

REFERENCES

Boyles, C. A. "Theory of Compliant Tube Luneburg Lens." J. Acoustical Society of America, 61:338, 1977.

Byron, E. V. "Low Sidelobe Response by Combining Hydrophones on an Acoustic Luneburg Lens." Eighth International Congress on Acoustics, London, 1974. (Goldcrest, Trowbridge, Willshire)

Elliott, R. S. Antenna Theory and Design. Prentice-Hall, 1981.

Green, J. A. "Microphone Reflector Geometries for Laser/Acoustic Bathymetry." 6 June 1981.

Luneburg, R. K. Mathematical Theory of Optics. University of California Press, Los Angeles, California, 1964.

Rasmussen, J. "J. Acoustical Society of America." 68(1), July 1980.

SECURITY CLASSIFICATION OF THIS PAGE (When Data Entered)

REPORT DOCUMENTATION PAGE		READ INSTRUCTIONS BEFORE COMPLETING FORM
1 REPORT NUMBER AST-R-151181	2 GOVT ACCESSION NO. ADA110 872	3 RECIPIENT'S CATALOG NUMBER
4 TITLE (and Subtitle) An Experimental Facility for Laser/ Acoustic Applications		5 TYPE OF REPORT & PERIOD COVERED Interim 6 PERFORMING ORG REPORT NUMBER
7 AUTHOR(s) G. Daniel Hickman John A. Edmonds		8 CONTRACT OR GRANT NUMBER(s) N00014-78-C-0764
9 PERFORMING ORGANIZATION NAME AND ADDRESS Applied Science Technology, Inc. 1011 Arlington Blvd., Suite 317 Arlington, VA 22209		10 PROGRAM ELEMENT, PROJECT, TASK AREA & WORK UNIT NUMBERS
11 CONTROLLING OFFICE NAME AND ADDRESS Office of Naval Research Coastal Sciences, Code 422CS Arlington, VA 22217		12 REPORT DATE November 1981 13 NUMBER OF PAGES 64
14 MONITORING AGENCY NAME & ADDRESS(if different from Controlling Office) Office of Naval Research Coastal Sciences, Code 422CS Arlington, VA 22217		15 SECURITY CLASS (of this report) Unclassified 15a DECLASSIFICATION DOWNGRADING SCHEDULE

16 DISTRIBUTION STATEMENT (of this Report)

Approved public release; distribution unlimited.

17 DISTRIBUTION STATEMENT (of the abstract entered in Block 20, if different from Report)

18 SUPPLEMENTARY NOTES

19 KEY WORDS (Continue on reverse side if necessary and identify by block number)

CO_2 Laser	Trafficability
Acoustics	Mines
Bathymetry	Remote Sensing
Soil Moisture	

20 ABSTRACT (Continue on reverse side if necessary and identify by block number)

This report describes the Experimental Laser/Acoustic System (ELAS) developed by Applied Science Technology, Inc., for applications involving the CO_2 laser/acoustic technique. This system is composed of a) a CO_2 laser transmitter to generate the acoustic signals in water, b) an acoustic receiving system, c) signal recording and analysis equipment, and d) a computer. A detailed description has been given for each of these subsystems.

DD FORM 1 JAN 73 1473 EDITION OF 1 NOV 65 IS OBSOLETE
S/N 0102-LF-014-6601

Unclassified
SECURITY CLASSIFICATION OF THIS PAGE (When Data Entered)

Laboratory and field measurements have used this system to investigate the feasibility of the laser/acoustic technique for remote sensing applications of a) shallow turbid water bathymetry, b) underwater object (mine) detection, and c) soil moisture determination. The ELAS is an extremely versatile system as it is not tied to any specific transmitter or sensors. Therefore, there are numerous other applications involved with navigation and communication which this system could be used to investigate. Brief summaries of results obtained on the bathymetry, mine, and soil moisture programs are included.

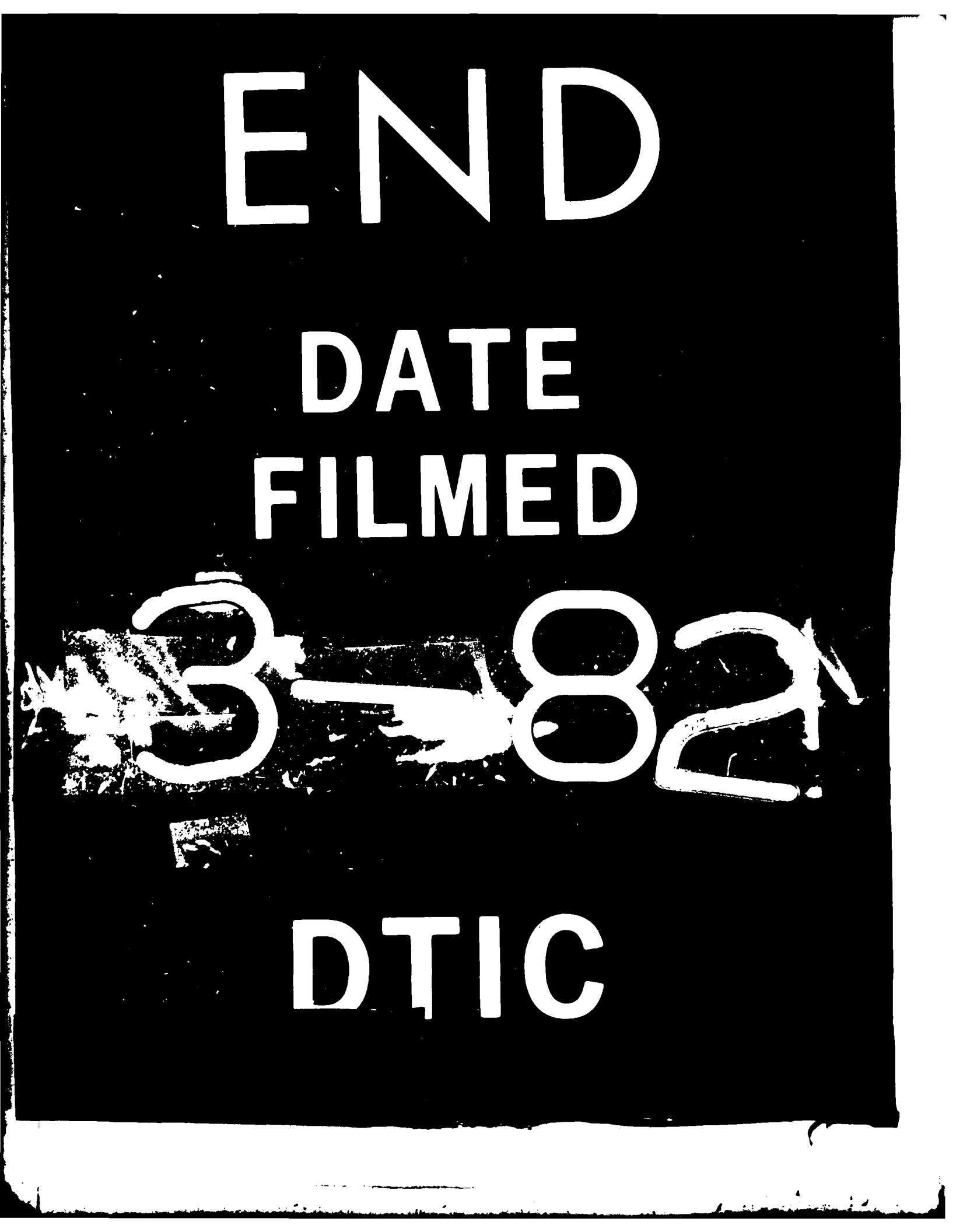
END
DATE
FILMED
3-82
DTIC